TU Delft

Delft University of Technology

Document Version
Final published version

Licence
CC BY

Citation (APA)
Manni, C., Speleers, H., & Toshniwal, D. (2026). Isogeometric discrete differential forms with Tchebycheffian B-splines. *Journal of Computational Physics*, *566*, Article 115195. https://doi.org/10.1016/j.jcp.2026.115195

Important note
To cite this publication, please use the final published version (if applicable).
Please check the document version above.

Copyright
In case the licence states “Dutch Copyright Act (Article 25fa)”, this publication was made available Green Open Access via the TU Delft Institutional Repository pursuant to Dutch Copyright Act (Article 25fa, the Taverne amendment). This provision does not affect copyright ownership.
Unless copyright is transferred by contract or statute, it remains with the copyright holder.

Sharing and reuse
Other than for strictly personal use, it is not permitted to download, forward or distribute the text or part of it, without the consent of the author(s) and/or copyright holder(s), unless the work is under an open content license such as Creative Commons.

Takedown policy
Please contact us and provide details if you believe this document breaches copyrights.
We will remove access to the work immediately and investigate your claim.

This work is downloaded from Delft University of Technology.

Journal of Computational Physics 566 (2026) 115195

Contents lists available at ScienceDirect

Journal of Computational Physics

journal homepage: www.elsevier.com/locate/jcp

Isogeometric discrete differential forms with Tchebycheffian B-splines

Carla Manni [a], Hendrik Speleers [a], Deepesh Toshniwal [b,*]

[a] Department of Mathematics, University of Rome Tor Vergata, Italy
[b] Delft Institute of Applied Mathematics, Delft University of Technology, The Netherlands

ARTICLE INFO

Keywords:
Isogeometric analysis
Tchebycheffian B-splines
Differential forms
de Rham complex
Finite element exterior calculus

ABSTRACT

We propose and analyze discretizations of the de Rham complex built from Tchebycheffian B-splines (TB-splines). In particular, we present a unified theoretical framework for approximating scalar and vector fields in mixed isogeometric methods using TB-spline spaces whose local pieces lie in the nullspaces of suitable constant-coefficient linear differential operators. This construction enriches the classical polynomial spline spaces by incorporating trigonometric and exponential shape functions while preserving key features of polynomial B-splines (e.g., local support, partition of unity, stable bases) and avoiding the limitations of rational (NURBS) models. For one-, two- and three-dimensional settings, we construct TB-spline de Rham complexes together with bounded commuting projections. The spaces in the resulting discrete complexes enable robust discretizations of mixed scalar and vector Laplacians, the Maxwell eigenvalue problem, and others. We also provide numerical experiments illustrating optimal approximation rates, spectrally-correct solutions to the Maxwell eigenvalue problem, and an application to incompressible flows. These tests validate the theory and demonstrate the practical advantages of TB-splines over purely polynomial constructions.

1. Introduction

The well-posedness of many partial differential problems reflects the underlying geometrical, topological and algebraic structures of the problem, as formalized by exterior calculus, Hodge theory, and homological algebra. It is well understood that, to avoid spurious behavior, instability, or non-physical solutions, numerical methods designed for their approximation must be structure-preserving. This means that they must reproduce or mimic the underlying structures of the problem at the discrete level, rather than merely approximate them. In several important applications, such as electromagnetism, this compatibility is primarily related to elliptic complexes, mostly the de Rham complex [1].

Within the powerful framework of isogeometric analysis [2], discretizations of differential forms based on tensor-product polynomial splines that satisfy a de Rham diagram have been proposed in [3,4]; see also [5,6]. Their approximation and stability properties have been thoroughly analyzed, and their effectiveness in practical applications – such as the Maxwell eigenvalue problem – has been demonstrated through numerous numerical experiments. More recently, extensions to adaptively-refinable spaces have been proposed and studied in [7–10] using hierarchical splines.

Extended Tchebycheff (ET) spaces are natural generalizations of algebraic polynomial spaces, in the sense that any non-trivial element of an ET-space of dimension $p+1$ has at most p zeros, counted with multiplicity. Extended complete Tchebycheff (ECT)

* Corresponding author.
E-mail addresses: manni@mat.uniroma2.it (C. Manni), speleers@mat.uniroma2.it (H. Speleers), d.toshniwal@tudelft.nl (D. Toshniwal).

https://doi.org/10.1016/j.jcp.2026.115195
Received 21 February 2026; Received in revised form 1 July 2026; Accepted 8 July 2026
Available online 10 July 2026
0021-9991/© 2026 The Authors. Published by Elsevier Inc. This is an open access article under the CC BY license (http://creativecommons.org/licenses/by/4.0/).

spaces form a particularly interesting subclass of ET-spaces. Notable examples include nullspaces of linear differential operators with constant coefficients defined over suitable intervals [11–14]. With some abuse of notation we will refer to p as the degree of an ECT-space to stress the similarity with polynomials. ECT-spaces enable a natural yet powerful generalization of classical polynomial splines: Tchebycheffian splines, which are smooth, piecewise-defined functions whose pieces are drawn from ECT-spaces.

Under suitable assumptions on the underlying ECT-spaces, Tchebycheffian splines admit a representation in terms of basis functions called Tchebycheffian B-splines (TB-splines). These basis functions enjoy almost all the properties that make polynomial B-splines popular and successful, including local linear independence, local support, non-negativity, and partition of unity. A multivariate extension of TB-splines can be readily achieved using the standard tensor-product approach. Moreover, local tensor-product structures that support local refinement – such as hierarchical splines and LR-splines – extend naturally to the Tchebycheffian setting [15,16].

TB-splines whose segments belong to ECT-spaces defined as nullspaces of constant-coefficient linear differential operators offer a rich variety of combinations involving algebraic polynomials, exponential functions, and trigonometric functions, equipped with a wide range of shape parameters. Moreover, they can be easily integrated into any software library that supports polynomial B-splines, thanks to the development of efficient routines for their evaluation and manipulation; we refer the interested reader to the (open-source) implementation available in [17] based on the results in [18]. Hence, this subclass of TB-splines provides a valid alternative to classical polynomial B-splines and their rational extension (NURBS) within the isogeometric paradigm. As demonstrated in [15,16,19–21], they can outperform (local) tensor-product polynomial B-splines in isogeometric Galerkin and collocation methods, particularly when appropriate problem-driven selection strategies for the underlying ECT-spaces are employed.

Unlike NURBS, Tchebycheffian splines whose pieces belong to nullspaces of constant-coefficient linear differential operators (containing constant functions) enjoy the same simple behavior under differentiation as polynomial splines: their derivatives are themselves Tchebycheffian splines, defined piecewise over the same types of spaces, but with the degree reduced by one. This additional structural similarity with polynomial splines paves the path towards a natural extension of the classical polynomial framework in the design of structure-preserving isogeometric discretization methods.

In this paper, we present and analyze discretizations of differential forms based on TB-splines, where the individual pieces are drawn from nullspaces of constant-coefficient linear differential operators (containing constant and linear functions). Specifically, we construct Tchebycheffian spline discretization spaces and the corresponding projection operators that satisfy a commuting de Rham diagram in two and three spatial dimensions. Our results extend the framework established in [3,4]. As demonstrated by the numerical experiments, the richness of TB-splines can feature more accurate approximations per degree of freedom – particularly when suitable, problem-driven automatic selection strategies for the underlying ECT-spaces are employed.

The remainder of the paper is divided into five sections. In Section 2 we briefly summarize the definition and main properties of ECT-spaces and TB-splines, with a special focus on nullspaces of constant-coefficient linear differential operators. In Section 3 we present the construction of Tchebycheffian spline spaces and corresponding projectors verifying a commuting univariate de Rham diagram, which are the building blocks of the bivariate and trivariate constructions presented in Section 4. Section 5 uses the structure-preserving isogeometric analysis package `Mantis.jl` [22] to simulate some classical numerical examples with TB-spline de Rham complexes, to validate the theoretical findings. Finally, Section 6 ends the paper with some concluding remarks.

Throughout the paper, we adopt the same notation as in [3] for spaces. For a bounded Lipschitz domain $\Omega \subset \mathbb{R}^d$, we denote by $L^2(\Omega)$ the usual space of square integrable functions on Ω equipped with the standard L^2-norm and by $\mathbf{L}^2(\Omega)$ its vectorial counterpart. Similarly, $H^s(\Omega)$ denotes the Hilbert space of functions in $L^2(\Omega)$ with derivatives up to order s in $L^2(\Omega)$ and $\mathbf{H}^s(\Omega)$ will again denote its vectorial counterpart. Moreover, we denote by $\mathbf{H}^s(\mathbf{curl};\Omega)$ the space of all functions in $\mathbf{H}^s(\Omega)$ such that their curl also belongs to $\mathbf{H}^s(\Omega)$. Similarly, $\mathbf{H}^s(\mathrm{div};\Omega)$ denotes the space of all functions in $\mathbf{H}^s(\Omega)$ such that their divergence also belongs to $H^s(\Omega)$. As is common in the literature, we drop the index when $s = 0$.

2. The Tchebycheff setting

In order for the paper to be self-contained, in this section we briefly summarize the definition and main properties of Tchebycheffian splines and B-splines we are going to use in the rest of the paper. We follow the notation from [21]. We refer the interested reader to [12,14,21,23] and references therein for more details and proofs.

2.1. Extended complete Tchebycheff spaces

Extended Tchebycheff spaces are $(p+1)$-dimensional spaces that are a natural extension of the space of algebraic polynomials of degree less than or equal to p.

Definition 1 (Extended Tchebycheff space)**.** Given an interval J and an integer $p \geq 0$, a space $\mathbb{T}_p(J) \subset C^p(J)$ of dimension $p+1$ is an extended Tchebycheff (ET) space on J if any non-trivial element vanishes at most p times (counting multiplicity) in J.

If J is closed and bounded, ET-spaces possess an additional property that strengthens the similarity with algebraic polynomials even further. For any ET-space $\mathbb{T}_p(J)$ on a bounded and closed interval J, there exist functions $g_0, \dots, g_p$ such that $\mathbb{T}_p(J) = \langle g_0, \dots, g_p \rangle$ and every subspace $\langle g_0, \dots, g_k \rangle$ for $k = 0, \dots, p$ is an ET-space on J. In this case, $\mathbb{T}_p(J)$ is called an extended complete Tchebycheff (ECT) space on J and the basis $\{g_0, \dots, g_p\}$ is called an ECT-system. A space $\mathbb{T}_p(J) \subset C^p(J)$ of dimension $p+1$ is an ECT-space on J if and

only if there exist positive functions $w_j \in C^{p-j}(J)$, $j = 0, 1, \dots, p$, such that $\mathbb{T}_p(J)$ is spanned by the following functions [11]:

$$\begin{cases} g_0(x) := w_0(x), \\ g_1(x) := w_0(x) \int_z^x w_1(y_1)\mathrm{d}y_1, \\ \qquad \vdots \\ g_p(x) := w_0(x) \int_z^x w_1(y_1) \int_z^{y_1} \dots \int_z^{y_{p-1}} w_p(y_p)\mathrm{d}y_p\mathrm{d}y_{p-1} \dots \mathrm{d}y_1, \end{cases} \tag{1}$$

where z is any point in J. The functions $g_0, \dots, g_p$ are called generalized power functions, the functions $w_0, \dots, w_p$ are usually referred to as weights, and the collection $\{w_0, \dots, w_p\}$ is called a weight system generating $\mathbb{T}_p(J)$. A given ECT-space on an interval J can be generated by different weight systems.

Example 1. The space of algebraic polynomials $\mathbb{P}_p = \langle 1, x, \dots, x^p \rangle$ is an ECT-space on the real line. A weight system for $\mathbb{P}_p$ is obtained by taking $w_j = 1$, $j = 0, \dots, p$. Indeed, with any fixed point $z \in \mathbb{R}$, through (1) these weights provide the basis

$$\left\{ 1, x - z, \frac{(x-z)^2}{2}, \dots, \frac{(x-z)^p}{p!} \right\}. \tag{2}$$

When dealing with ECT-spaces, it is often convenient to replace the usual derivatives by some related differential operators identified by the weights. We define $D_0 f := f$ and

$$D_j f := \partial\left(\frac{f}{w_{j-1}} \right), \quad j = 1, \dots, p+1, \tag{3}$$

and we set

$$L_j := D_j D_{j-1} \dots D_0, \quad j = 0, \dots, p+1. \tag{4}$$

Note that the ECT-space $\mathbb{T}_p(J)$ generated by $\{w_0, \dots, w_p\}$ is the nullspace of L_{p+1}.

In the paper we will confine ourselves to a large class of ECT-spaces: the nullspaces of linear differential operators with real constant coefficients. More precisely, let us consider the differential operator defined by

$$\mathcal{L}_p f := \partial^{p+1} f + \sum_{j=0}^{p} a_j \partial^j f, \quad f \in C^{p+1}(\mathbb{R}), \quad a_j \in \mathbb{R}, \quad j = 0, \dots, p, \tag{5}$$

whose characteristic polynomial

$$\mathfrak{p}_p(\omega) := \omega^{p+1} + \sum_{j=0}^{p} a_j \omega^j \tag{6}$$

has roots $\omega_k = \alpha_k + \mathrm{i}\beta_k$ ($\alpha_k, \beta_k \in \mathbb{R}$ and $\mathrm{i} := \sqrt{-1}$) of multiplicity $\mu_k \geq 1$, with $k = 0, \dots, M$, such that $\sum_{k=0}^{M} \mu_k = p+1$, and $\omega_0 = 0$. The nullspace of $\mathcal{L}_p$ is formed by the full collection of the following subspaces associated with the roots of the polynomial in (6): for $k = 0, \dots, M$,

$$\left\langle x^l e^{\alpha_k x} : l = 0, \dots, \mu_k - 1 \right\rangle \quad \text{if } \beta_k = 0,$$

and

$$\left\langle x^l e^{\alpha_k x} \cos(\beta_k x), x^l e^{\alpha_k x} \sin(\beta_k x) : l = 0, \dots, \mu_k - 1 \right\rangle \quad \text{if } \beta_k \neq 0.$$

The nullspace of $\mathcal{L}_p$ is an ECT-space on a suitable interval $[a, b]$ and such a property is invariant under translation of the interval. In particular, if $\mathfrak{p}_p$ has only real roots, then the nullspace is an ECT-space on the real line. Otherwise, the interval is bounded and its length depends on the (complex) roots of $\mathfrak{p}_p$. More precisely, the nullspace of $\mathcal{L}_p$ is an ECT-space at least on any interval $[a, b]$ such that

$$b - a < \frac{\pi}{\mathfrak{M}}, \tag{7}$$

where $\mathfrak{M} \geq 0$ is the maximum of the imaginary parts of all roots of the characteristic polynomial.

The nullspace of $\mathcal{L}_p$ will be denoted by $\mathbb{P}_p^{\mathcal{W}}$, where

$$\mathcal{W} := \Big(\underbrace{\omega_1, \dots, \omega_1}_{\mu_1 \text{ times}}, \underbrace{\omega_2, \dots, \omega_2}_{\mu_2 \text{ times}}, \dots, \underbrace{\omega_M, \dots, \omega_M}_{\mu_M \text{ times}} \Big), \tag{8}$$

which is a vector with $p + 1 - \mu_0$ components and uniquely characterizes the nullspace. In the following, we will refer to p as the degree of $\mathbb{P}_p^{\mathcal{W}}$ and assume that $\mu_0 \geq 2$, to ensure the considered space contains constant and linear functions.

Remark 1. ECT-spaces $\mathbb{P}_p^{\mathcal{W}}$ offer great flexibility through their shape parameters, namely the roots of the characteristic polynomial in (8). A particular selection of these shape parameters results in familiar subclasses of ECT-spaces, such as algebraic polynomials:

$$\mathbb{P}_p = \langle 1, x, \dots, x^p \rangle,$$

or instances of generalized polynomial spaces [19,20]:

$$\mathbb{P}_p^{(\alpha,-\alpha)} = \left\langle 1, x, \dots, x^{p-2}, e^{\alpha x}, e^{-\alpha x} \right\rangle = \left\langle 1, x, \dots, x^{p-2}, \cosh(\alpha x), \sinh(\alpha x) \right\rangle, \quad p \geq 3, \tag{9}$$

$$\mathbb{P}_p^{(\mathrm{i}\beta,-\mathrm{i}\beta)} = \left\langle 1, x, \dots, x^{p-2}, \cos(\beta x), \sin(\beta x) \right\rangle, \quad p \geq 3. \tag{10}$$

All the above examples are special instances of

$$\mathbb{P}_p^{(\alpha_1,\dots,\alpha_\ell,\mathrm{i}\beta_1,-\mathrm{i}\beta_1,\dots,\mathrm{i}\beta_q,-\mathrm{i}\beta_q)} = \left\langle 1, x, \dots, x^{p-\ell-2q}, e^{\alpha_1 x}, \dots, e^{\alpha_\ell x}, \cos(\beta_1 x), \sin(\beta_1 x), \dots, \cos(\beta_q x), \sin(\beta_q x) \right\rangle, \tag{11}$$

defined on a reference interval ensuring the ECT-property. The features of the ECT-spaces (11) in isogeometric Galerkin discretizations have been investigated in [21].

Remark 2. For $p \geq 1$, let $\mathbb{T}_p$ be a space of dimension $p+1$ on J. Assume that the derivative space of $\mathbb{T}_p$, i.e., the space spanned by the derivatives of functions in $\mathbb{T}_p$, is a p-dimensional ECT-space on the interval J generated by the weight system $\{w_1, \dots, w_p\}$. Then, from (1) it follows that $\mathbb{T}_p$ is a $(p+1)$-dimensional ECT-space on J generated by the weight system $\{1, w_1, \dots, w_p\}$. In particular, it can be easily checked that the derivative space of $\mathbb{P}_p^{\mathcal{W}}$ is $\mathbb{P}_{p-1}^{\mathcal{W}}$. In other words, the derivative space of $\mathbb{P}_p^{\mathcal{W}}$ is an ECT-space with the same structure, of degree $p-1$. If the weight system $\{w_1, \dots, w_p\}$ generates the derivative space on J, then $\{1, w_1, \dots, w_p\}$ is a weight system for $\mathbb{P}_p^{\mathcal{W}}$ on J.

2.2. Tchebycheffian spline spaces and Tchebycheffian B-splines

In complete similarity with polynomial splines, Tchebycheffian splines are piecewise functions with pieces belonging to ECT-spaces, glued together with certain prescribed smoothness. A full Tchebycheffian spline theory has been developed for splines where the various pieces are taken from different and general Tchebycheff spaces; see [12,14,21,23] and references therein. However, for the sake of simplicity, we limit ourselves to spaces where the different pieces belong to the same ECT-space of the form $\mathbb{P}_p^{\mathcal{W}}$ because they already offer a large variety of shape parameters to be profitably used in applications and possess a structure with respect to differentiation (see Remark 2), which is particularly well suited for the construction of discrete de Rham complexes we are aiming for.

More precisely, let Δ be a partition of the interval $[a,b] \subset \mathbb{R}$ specified in terms of a sequence of breakpoints,

$$\Delta := \{a =: \eta_0 < \eta_1 < \dots < \eta_{m-1} < \eta_m := b\}.$$

We set $J_i := [\eta_{i-1}, \eta_i)$, $i = 1, \dots, m-1$, and $J_m := [\eta_{m-1}, \eta_m]$. Finally, let us consider a sequence of $m-1$ integers,

$$\mathbf{r} := \{r_i \in \mathbb{Z} : -1 \leq r_i \leq p-1,\ i = 1, \dots, m-1\}.$$

Let $\mathbb{P}_p^{\mathcal{W}}$ be an ECT-space on $[a,b]$, the elements of the set

$$\begin{aligned} \mathbb{S}_p^{\mathbf{r}}(\Delta, \mathcal{W}) := \big\{ f : [a,b] \to \mathbb{R} : f|_{J_i} \in \mathbb{P}_p^{\mathcal{W}},\ i = 1, \dots, m; \\ \partial_-^l f(\eta_i) = \partial_+^l f(\eta_i),\ l = 0, \dots, r_i,\ i = 1, \dots, m-1 \big\} \end{aligned} \tag{12}$$

are Tchebycheffian splines of degree p and smoothness $\mathbf{r}$ on the partition Δ of the interval $[a,b]$, related to $\mathbb{P}_p^{\mathcal{W}}$. The dimension of the space $\mathbb{S}_p^{\mathbf{r}}(\Delta, \mathcal{W})$ is given by

$$n := p + 1 + \sum_{i=1}^{m-1} (p - r_i). \tag{13}$$

We can construct a basis for the space $\mathbb{S}_p^{\mathbf{r}}(\Delta, \mathcal{W})$ that possesses all the characterizing properties of the standard polynomial B-splines. These basis functions will be referred to as Tchebycheffian B-splines (TB-splines) and denoted by

$$\left\{ N_{k,p}^{\mathcal{W}} : k = 1, \dots, n \right\}.$$

Similar to polynomial B-splines, TB-splines can be defined using a vector of non-decreasing (open) knots,

$$\Xi := (\xi_k)_{k=1}^{n+p+1} := \Big(\underbrace{\eta_0, \dots, \eta_0}_{p+1 \text{ times}}, \underbrace{\eta_1, \dots, \eta_1}_{p-r_1 \text{ times}}, \dots, \underbrace{\eta_{m-1}, \dots, \eta_{m-1}}_{p-r_{m-1} \text{ times}}, \underbrace{\eta_m, \dots, \eta_m}_{p+1 \text{ times}} \Big). \tag{14}$$

Definition 2 (TB-splines)**.** Let $\{w_0, w_1, \dots, w_p\}$, with $w_0 = 1$, be a weight system generating $\mathbb{P}_p^{\mathcal{W}}$ on $[a,b]$. Given the knot vector (14), the TB-splines $\{N_{k,p}^{\mathcal{W}} : k = 1, \dots, n\}$ are defined recursively as follows [12]: for $x \in [a,b)$, $q = 0, \dots, p$ and $k = 1, \dots, n+p-q$,

$$N_{k,0}^{\mathcal{W}}(x) := \begin{cases} w_p(x), & x \in [\xi_k, \xi_{k+1}), \\ 0, & \text{otherwise}, \end{cases}$$

and

$$N_{k,q}^{\mathcal{W}}(x) := w_{p-q}(x) \int_a^x \left[\frac{N_{k,q-1}^{\mathcal{W}}(y)}{\gamma_{k,q-1}} - \frac{N_{k+1,q-1}^{\mathcal{W}}(y)}{\gamma_{k+1,q-1}} \right] \mathrm{d}y, \quad q > 0,$$

where

$$\gamma_{j,l} := \int_a^b N_{j,l}^{\mathcal{W}}(y)\,\mathrm{d}y,$$

and if $\gamma_{j,l} = 0$ then

$$\int_a^x \frac{N_{j,l}^{\mathcal{W}}(y)}{\gamma_{j,l}}\,\mathrm{d}y := \begin{cases} 1, & x \geq \xi_{j+l+1}, \\ 0, & \text{otherwise.} \end{cases}$$

At the end-point b, the spline $N_{k,q}^{\mathcal{W}}$ is defined by taking the limit from the left, i.e., $N_{k,q}^{\mathcal{W}}(b) := \lim_{x\to b-} N_{k,q}^{\mathcal{W}}(x)$.

TB-splines exhibit a complete structural similarity with polynomial B-splines. In particular, they enjoy the nice properties collected in the following proposition; see [12,23] and references therein.

Proposition 1. *Let $\{N_{k,p}^{\mathcal{W}} : k = 1,\dots,n\}$ be the functions in Definition 2. Then,*

$$\mathbb{S}_p^{\mathbf{r}}(\Delta,\mathcal{W}) = \left\langle N_{k,p}^{\mathcal{W}} : k = 1,\dots,n \right\rangle,$$

and the following properties hold.

- *Non-negativity: $N_{k,p}^{\mathcal{W}}(x) > 0$ for all $x \in (\xi_k, \xi_{k+p+1})$;*
- *Local support: $N_{k,p}^{\mathcal{W}}(x) = 0$ for all $x \notin [\xi_k, \xi_{k+p+1}]$;*
- *Partition of unity: $\sum_{k=1}^{n} N_{k,p}^{\mathcal{W}}(x) = 1$ for all $x \in [a,b]$;*
- *Local linear independence: let $\xi_j < \xi_{j+1}$, then the set $\{N_{k,p}^{\mathcal{W}}\}_{k=j-p}^{j}$ forms a basis of $\mathbb{P}_p^{\mathcal{W}}$ on J_{i_j+1} for all $p+1 \leq j \leq n$, where i_j denotes the index such that $\xi_j = \eta_{i_j}$;*
- *Interpolation at end-points:*

$$N_{1,p}^{\mathcal{W}}(a) = 1, \quad N_{k,p}^{\mathcal{W}}(a) = 0, \quad k = 2,\dots,n,$$
$$N_{n,p}^{\mathcal{W}}(b) = 1, \quad N_{k,p}^{\mathcal{W}}(b) = 0, \quad k = 1,\dots,n-1;$$

- *Derivative formula:*

$$\partial N_{k,p}^{\mathcal{W}}(x) = M_{k-1,p-1}^{\mathcal{W}}(x) - M_{k,p-1}^{\mathcal{W}}(x),$$

where

$$M_{k,p-1}^{\mathcal{W}}(x) := \frac{N_{k+1,p-1}^{\mathcal{W}}(x)}{\gamma_{k+1,p-1}},$$

with $M_{0,p-1}^{\mathcal{W}}(x) = M_{n,p-1}^{\mathcal{W}}(x) = 0$.

From now on, we assume $p \geq 1$ and $\mathbf{r} \geq \mathbf{0}$ (i.e., $r_i \geq 0$ for $i = 1,\dots,m-1$), so that the elements of $\mathbb{S}_p^{\mathbf{r}}(\Delta,\mathcal{W})$ are at least continuous in $[a,b]$. From Remark 2 we know that the derivative of any element of $\mathbb{S}_p^{\mathbf{r}}(\Delta,\mathcal{W})$ belongs to $\mathbb{S}_{p-1}^{\mathbf{r}-\mathbf{1}}(\Delta,\mathcal{W})$. Moreover, the application

$$\partial : \mathbb{S}_p^{\mathbf{r}}(\Delta,\mathcal{W}) \to \mathbb{S}_{p-1}^{\mathbf{r}-\mathbf{1}}(\Delta,\mathcal{W}) \tag{15}$$

is surjective. Under the assumption that the root vector w is such that $\mu_0 \geq 2$ (and $w_0 = w_1 = 1$), we have

$$x = \sum_{k=1}^{n} \xi_{k,p}^{*,\mathcal{W}} N_{k,p}^{\mathcal{W}}(x), \quad \forall x \in [a,b]. \tag{16}$$

The coefficients $\xi_{k,p}^{*,\mathcal{W}}$ are called (Tchebycheffian) Greville abscissae. It holds that

$$\xi_{k,p}^{*,\mathcal{W}} \in [\xi_{k+1}, \xi_{k+p}].$$

Moreover, all $\xi_{k,p}^{*,\mathcal{W}}$ are distinct and define a partition of $[a,b]$. This is in complete analogy with the polynomial case.

Remark 3. In our definition of Tchebycheffian splines (12) we assume that $\mathbb{P}_p^{\mathcal{W}}$ is a $(p+1)$-dimensional ECT-space on the whole interval $[a,b]$. This assumption can be restrictive if $\mathbb{P}_p^{\mathcal{W}}$ includes trigonometric functions because upper bounds for $b-a$ are required; see (7). However, the assumption has been stated just to keep the presentation as simple as possible but it is not an issue in practice. Indeed, if $\mathbb{P}_p^{\mathcal{W}}$ is an ECT-space on intervals of length less than $b-a$, then the space $\mathbb{S}_p^{\mathbf{r}}(\Delta,\mathcal{W})$ is still well defined and it admits a TB-spline basis when the derivative space of $\mathbb{P}_p^{\mathcal{W}}$ (see Remark 2) is an ECT-space on each interval $[\xi_{k+1}, \xi_{k+p}]$, where $\xi_{k+1} < \xi_{k+p}$ and $1 \leq k \leq n$; see [24] (and also [25] for the case of trigonometric B-splines). Note that these intervals are closely related to the supports of the TB-splines; see Proposition 1. Therefore, when dealing with nullspaces of constant-coefficient linear differential operators, a TB-spline basis for $\mathbb{S}_p^{\mathbf{r}}(\Delta,\mathcal{W})$ always exists provided that a sufficiently fine partition of $[a,b]$ is considered (just the weight system in Definition 2 has to be properly modified; see [18]). Sufficient conditions on the maximal size of the elements can be immediately deduced from (7).

Remark 4. The recurrence relation in Definition 2 is an important theoretical tool to define and analyze TB-splines, but it is of limited practical interest because it does not lead to an efficient evaluation strategy. Efficient routines to construct and manipulate TB-splines with pieces belonging to ECT-spaces of the form $\mathbb{P}_p^{\mathcal{W}}$ have been provided in [17] by implementing the approach described in [18]. The TB-spline construction procedure developed in [17,18] does not require any knowledge about weight systems of $\mathbb{P}_p^{\mathcal{W}}$. It just requires that $\mathbb{P}_p^{\mathcal{W}}$ is an ECT-space on each J_i, $i = 1, \dots, m$. If $\mathbb{P}_p^{\mathcal{W}}$ is not an ECT-space on $[a, b]$ and the partition Δ is not fine enough (see Remark 3), then the procedure simply returns a sequence of functions that might not enjoy the properties listed in Proposition 1. Although the evaluation of TB-splines for extreme values of the shape parameters (i.e., the roots of the characteristic polynomial (6)), high degrees, high smoothness, and highly non-uniform partitions still faces numerical challenges [17], the above mentioned routines provide reliable tools for a large class of TB-splines of interest in practical applications. A Matlab implementation is available through the ACM Collected Algorithms (CALGO) library [17]. A Julia implementation based on [17] is available in the structure-preserving isogeometric analysis package `Mantis.jl` [22], which has been used to perform the numerical tests in Section 5. An alternative evaluation strategy has been proposed in [26] but no implementation is available.

3. Univariate Tchebycheffian discrete de Rham complex

In this section we provide the univariate building blocks to be used later for the construction of Tchebycheffian isogeometric discrete differential forms in two and three dimensions. We first introduce suitable projectors onto the spline space $\mathbb{S}_p^{\mathbf{r}}(\Delta, w)$ and its derivative space, and we analyze their stability and approximation properties. Afterwards, we use them to build a discrete univariate de Rham complex based on Tchebycheffian splines.

3.1. Commuting stable projectors onto Tchebycheffian spline spaces

We assume that the partition Δ is quasi-uniform, i.e.,

$$\frac{\max_{i=1,\dots,m}(\eta_i - \eta_{i-1})}{\min_{i=1,\dots,m}(\eta_i - \eta_{i-1})}$$

is bounded by a constant independent of m, and we set

$$h_\Delta := \max_{i=1,\dots,m} (\eta_i - \eta_{i-1}).$$

For a given Tchebycheffian spline space $\mathbb{S}_p^{\mathbf{r}}(\Delta, w)$, we consider the functionals $\{\lambda_k : k = 1, \dots, n\}$ constructed in [14, Eq. (9.64)]. Then, for any $f \in L^1(a, b)$, we define the spline quasi-interpolant

$$\widehat{\Pi}_p^{\mathcal{W}} f := \sum_{k=1}^{n} \lambda_k(f) N_{k,p}^{\mathcal{W}}. \tag{17}$$

This is a projector onto the spline space $\mathbb{S}_p^{\mathbf{r}}(\Delta, w)$, i.e., $\widehat{\Pi}_p^{\mathcal{W}} f = f$ for all $f \in \mathbb{S}_p^{\mathbf{r}}(\Delta, w)$. The projector in [5, Eq. (2.19)] is a special instance of (17) for the polynomial case, i.e., when $\mathbb{P}_p^{\mathcal{W}} = \mathbb{P}_p$.

We now deduce from [14, Chapter 9] two properties, which allow us to prove the stability of the operator in (17). In the following, C denotes a generic constant. We start with the following Markov-type inequality; see [14, Theorem 9.10].

Proposition 2. *For any $f \in \mathbb{P}_p^{\mathcal{W}}$ and $\xi_\ell < \xi_{\ell+1}$, we have*

$$\|\partial f\|_{L^2(\xi_\ell, \xi_{\ell+1})} \le \frac{C}{h_\Delta} \|f\|_{L^2(\xi_\ell, \xi_{\ell+1})},$$

where C is a constant depending only on p and w.

In addition, from [14, Theorem 9.26] we obtain the following result.

Proposition 3. *We have*

$$\|\lambda_k\| := \sup \frac{|\lambda_k(f)|}{\|f\|_{L^2(\xi_k, \xi_{k+p+1})}} \le \frac{C}{\sqrt{h_\Delta}}, \quad k = 1, \dots, n,$$

where C is a constant depending only on p and w.

This brings us to the following stability result, similar to [5, Proposition 2.2] in the polynomial case.

Proposition 4. *For any $\xi_\ell < \xi_{\ell+1}$ and $f \in L^2(a, b)$, we have*

$$\|\widehat{\Pi}_p^{\mathcal{W}} f\|_{L^2(\xi_\ell, \xi_{\ell+1})} \le C \|f\|_{L^2(\xi_{\ell-p}, \xi_{\ell+p+1})}, \tag{18}$$

and for $f \in H^1(a, b)$, we have

$$\|\partial \widehat{\Pi}_p^{\mathcal{W}} f\|_{L^2(\xi_\ell, \xi_{\ell+1})} \le C \|\partial f\|_{L^2(\xi_{\ell-p}, \xi_{\ell+p+1})}, \tag{19}$$

where C is a constant depending only on p and w.

Proof. From the support property of TB-splines we know that $N^{\mathcal{W}}_{k,p}$ is non-zero on the interval $[\xi_\ell, \xi_{\ell+1}]$ only for $k = \ell - p, \dots, \ell$. Moreover, using the non-negative partition of unity, we deduce

$$\|\widehat{\Pi}^{\mathcal{W}}_p f\|_{L^2(\xi_\ell,\xi_{\ell+1})} = \left\| \sum_{k=\ell-p}^{\ell} \lambda_k(f) N^{\mathcal{W}}_{k,p} \right\|_{L^2(\xi_\ell,\xi_{\ell+1})} \le \sqrt{h_\Delta} \max_{\ell-p\le k\le \ell} |\lambda_k(f)|.$$

Applying Proposition 3 immediately yields the inequality in (18).

Since $\widehat{\Pi}^{\mathcal{W}}_p$ is a projector onto $\mathbb{S}^{\mathbf{r}}_p(\Delta, w)$, it preserves, in particular, any constant $c \in \mathbb{R}$. Thus, from Proposition 2 we obtain

$$\|\partial \widehat{\Pi}^{\mathcal{W}}_p f\|_{L^2(\xi_\ell,\xi_{\ell+1})} = \|\partial \widehat{\Pi}^{\mathcal{W}}_p (f-c)\|_{L^2(\xi_\ell,\xi_{\ell+1})} \le \frac{C}{h_\Delta} \|\widehat{\Pi}^{\mathcal{W}}_p (f-c)\|_{L^2(\xi_\ell,\xi_{\ell+1})}.$$

Using (18) and a standard approximation estimate for constant functions gives

$$\|\partial \widehat{\Pi}^{\mathcal{W}}_p f\|_{L^2(\xi_\ell,\xi_{\ell+1})} \le \frac{C}{h_\Delta} \|f-c\|_{L^2(\xi_{\ell-p},\xi_{\ell+p+1})} \le \frac{C}{h_\Delta} (\xi_{\ell+p+1} - \xi_{\ell-p}) \|\partial f\|_{L^2(\xi_{\ell-p},\xi_{\ell+p+1})}.$$

It is clear that $\xi_{\ell+p+1} - \xi_{\ell-p} \le (2p+1)h_\Delta$ and thus (19) follows. □

Finally, from [14, Theorem 9.38] we know the following approximation result, which generalizes [5, Proposition 4.2] to the Tchebycheff setting.

Proposition 5. *For $f \in H^{p+1}(a,b)$, there exists a constant C such that*

$$\|\partial^j (f - \widehat{\Pi}^{\mathcal{W}}_p f)\|_{L^2(a,b)} \le C h_\Delta^{p+1-j} \|L_{p+1} f\|_{L^2(a,b)}, \quad j = 0, \dots, p,$$

where L_{p+1} is defined in (4).

In view of the de Rham complex we will consider later, we also define another spline quasi-interpolant. Given the projector $\widehat{\Pi}^{\mathcal{W}}_p$ described above, we define

$$\widehat{\Pi}^{c,\mathcal{W}}_{p-1} g(\hat{x}) := \partial \widehat{\Pi}^{\mathcal{W}}_p \int_a^{\hat{x}} g(y)\,\mathrm{d}y, \tag{20}$$

for all functions g such that $f(\hat{x}) = \int_a^{\hat{x}} g(y)\,\mathrm{d}y \in L^1(a,b)$ (or f is in the domain of $\widehat{\Pi}^{\mathcal{W}}_p$). The superscript c stands for *commuting* because, indeed, it is immediate to check that

$$\widehat{\Pi}^{c,\mathcal{W}}_{p-1} \partial f = \partial \widehat{\Pi}^{\mathcal{W}}_p f. \tag{21}$$

Since $\widehat{\Pi}^{\mathcal{W}}_p$ is a projector onto $\mathbb{S}^{\mathbf{r}}_p(\Delta, w)$, from (21) and (15) we deduce that the quasi-interpolant $\widehat{\Pi}^{c,\mathcal{W}}_{p-1}$ is a projector onto $\mathbb{S}^{\mathbf{r}-\mathbf{1}}_{p-1}(\Delta, w)$, the space of Tchebycheffian splines of degree $p-1$ and smoothness $\mathbf{r}-\mathbf{1}$ related to the ECT-space $\mathbb{P}^{\mathcal{W}}_{p-1}$.

By using (19) and (20) we arrive at the following stability result for $\widehat{\Pi}^{c,\mathcal{W}}_{p-1}$.

Proposition 6. *For any $\xi_\ell < \xi_{\ell+1}$ and $g \in L^2(a,b)$, we have*

$$\|\widehat{\Pi}^{c,\mathcal{W}}_{p-1} g\|_{L^2(\xi_\ell,\xi_{\ell+1})} \le C \|g\|_{L^2(\xi_{\ell-p},\xi_{\ell+p+1})}, \tag{22}$$

where C is a constant depending only on p and w.

From the approximation result for $\widehat{\Pi}^{\mathcal{W}}_p$ we obtain the following approximation result for $\widehat{\Pi}^{c,\mathcal{W}}_{p-1}$.

Proposition 7. *For $g \in H^p(a,b)$, there exists a constant C such that*

$$\|\partial^j (g - \widehat{\Pi}^{c,\mathcal{W}}_{p-1} g)\|_{L^2(a,b)} \le C h_\Delta^{p-j} \left\| L_{p+1} \int_a^{\hat{x}} g(y)\,\mathrm{d}y \right\|_{L^2(a,b)}, \quad j = 0, \dots, p-1, \tag{23}$$

where L_{p+1} is defined in (4).

Proof. Let $f(\hat{x}) = \int_a^{\hat{x}} g(y)\,\mathrm{d}y$. Then, by Proposition 5 we have

$$\begin{aligned} \|\partial^j (g - \widehat{\Pi}^{c,\mathcal{W}}_{p-1} g)\|_{L^2(a,b)} &= \|\partial^j (\partial f - \widehat{\Pi}^{c,\mathcal{W}}_{p-1} \partial f)\|_{L^2(a,b)} = \|\partial^j (\partial f - \partial \widehat{\Pi}^{\mathcal{W}}_p f)\|_{L^2(a,b)} \\ &= \|\partial^{j+1} (f - \widehat{\Pi}^{\mathcal{W}}_p f)\|_{L^2(a,b)} \le C h_\Delta^{p-j} \|L_{p+1} f\|_{L^2(a,b)}. \end{aligned}$$

This completes the proof. □

3.2. Univariate de Rham complex

The above results can now be used to construct the following commuting diagram. The top row is the continuous de Rham complex, the bottom row is the discrete de Rham complex built using Tchebycheffian splines, and the vertical arrows are L^2-stable commuting projectors:

$$\begin{array}{ccccccc} \mathbb{R} & \longrightarrow & H^1(a,b) & \xrightarrow{\partial} & L^2(a,b) & \longrightarrow & 0 \\ & & \downarrow{\scriptstyle \widehat{\Pi}^{\mathcal{W}}_p} & & \downarrow{\scriptstyle \widehat{\Pi}^{c,\mathcal{W}}_{p-1}} & & \\ \mathbb{R} & \longrightarrow & \mathbb{S}^{\mathbf{r}}_p(\Delta, w) & \xrightarrow{\partial} & \mathbb{S}^{\mathbf{r}-\mathbf{1}}_{p-1}(\Delta, w) & \longrightarrow & 0 \end{array} . \tag{24}$$

In particular, the exactness of the bottom row is due to the surjectivity of the application in (15). The commutativity of the diagram follows from (21).

The space $\mathbb{S}^{\mathbf{r}-\mathbf{1}}_{p-1}(\Delta, w)$ of Tchebycheffian splines of degree $p-1$ and smoothness $\mathbf{r}-\mathbf{1}$ related to the ECT-space $\mathbb{P}^{\mathcal{W}}_{p-1}$, can be represented in terms of the TB-splines $\{N^{\mathcal{W}}_{k,p-1} : k = 1, \dots, n-1\}$; see Proposition 1. However, to emphasize the role of $\mathbb{S}^{\mathbf{r}-\mathbf{1}}_{p-1}(\Delta, w)$ as derivative space of $\mathbb{S}^{\mathbf{r}}_{p}(\Delta, w)$, following [5] and [27], it is appropriate to use

$$\left\{M^{\mathcal{W}}_{k,p-1} : k = 1, \dots, n-1\right\} \tag{25}$$

as basis functions. Indeed, as in the polynomial case, from the derivative formula in Proposition 1, the bidiagonal lower triangular matrix representing the derivative is the same matrix representing the vertex-to-edge relation of the mesh in $[a, b]$ whose vertices are the (Tchebycheffian) Greville abscissae in (16), which are uniquely associated with the TB-splines $\{N^{\mathcal{W}}_{k,p} : k = 1, \dots, n\}$.

In the same spirit as the approach of [5, Proposition 2.4], from the derivative formula in Proposition 1, we obtain the following representation for $\widehat{\Pi}^{c,\mathcal{W}}_{p-1}$ with respect to the basis in (25):

$$\widehat{\Pi}^{c,\mathcal{W}}_{p-1} g = \sum_{k=1}^{n-1} \lambda^c_k(g) M^{\mathcal{W}}_{k,p-1},$$

where

$$\lambda^c_k(g) := \lambda_{k+1}\left(\int_{\xi_k}^{\widehat{x}} g(y)\,\mathrm{d}y\right) - \lambda_k\left(\int_{\xi_k}^{\widehat{x}} g(y)\,\mathrm{d}y\right).$$

The presented approach does not consider boundary conditions, but the constructions can be easily adapted to (homogeneous) boundary conditions as in the polynomial case; see [3, Section 3]. By the interpolation properties at the end-points in Proposition 1 we have that the TB-splines

$$\left\{N^{\mathcal{W}}_{k,p} : k = 2, \dots, n-1\right\}$$

form a basis for

$$\mathbb{S}^{\mathbf{r}}_{p,0}(\Delta, w) := \mathbb{S}^{\mathbf{r}}_{p}(\Delta, w) \cap H^1_0(a, b).$$

Therefore, to preserve homogeneous boundary conditions, the projector in (17) can be adapted as follows:

$$\widehat{\Pi}^{\mathcal{W}}_{p,0} f := \sum_{k=2}^{n-1} \lambda_k(f) N^{\mathcal{W}}_{k,p}, \tag{26}$$

and the projector in (20) can be adapted similarly. By recalling that the derivatives of functions in $H^1_0(a, b)$ are the functions in $L^2(a, b)$ with zero average and taking into account (15), we have that the following commuting de Rham diagram holds:

$$\begin{array}{ccccccc} 0 & \longrightarrow & H^1_0(a,b) & \xrightarrow{\partial} & L^2(a,b) & \xrightarrow{\int_a^b} & \mathbb{R} \\ & & \downarrow{\scriptstyle \widehat{\Pi}^{\mathcal{W}}_{p,0}} & & \downarrow{\scriptstyle \widehat{\Pi}^{c,\mathcal{W}}_{p-1,0}} & & \\ 0 & \longrightarrow & \mathbb{S}^{\mathbf{r}}_{p,0}(\Delta, w) & \xrightarrow{\partial} & \mathbb{S}^{\mathbf{r}-\mathbf{1}}_{p-1}(\Delta, w) & \xrightarrow{\int_a^b} & \mathbb{R} \end{array}. \tag{27}$$

4. Multivariate Tchebycheffian discrete de Rham complex

We now define our discretization spaces and projectors for two- and three-dimensional applications. In Sections 4.1 and 4.2 we present the discrete de Rham complexes on a unit cube, $\widehat{\Omega} := (0, 1)^d$, $d = 2, 3$. Then, for sufficiently regular and invertible geometric maps $\mathbf{F} : \widehat{\Omega} \to \Omega$, we briefly discuss in Section 4.3 how the discretizations on Ω can be handled.

Due to the complete structural similarity to the polynomial case, the extension to mapped domains can be performed following the same line of arguments as in [5], without any specific issue related to the Tchebycheff setting. Similarly, the stability and approximation properties of the univariate projectors allow us to obtain verbatim the full approximation results as in [3,5], both on parametric and mapped domains, and we skip the details here. For the same reason, we deliberately adopt, as much as possible, the same notation as in [3,5].

Let $(\mathbb{S}^{\mathbf{r}_l}_{p_l}(\Delta_l, w_l), \mathbb{S}^{\mathbf{r}_l-\mathbf{1}}_{p_l-1}(\Delta_l, w_l))$, $l = 1, \dots, d$ be pairs of univariate Tchebycheffian spline spaces forming d univariate discrete de Rham complexes as in (24), where Δ_l, $l = 1, \dots, d$ are the considered quasi-uniform partitions of the associated univariate domains $[0, 1]$. Variables and operators related to the parametric domain $\widehat{\Omega}$ are identified by a hat $\widehat{\cdot}$, while the same notation without a hat has the same meaning but related to the physical domain Ω.

4.1. Two-dimensional case

For $\widehat{\Omega} := (0, 1)^2$, we set

$$\widehat{\mathbb{X}}^0 := H^1(\widehat{\Omega}), \quad \widehat{\mathbb{X}}^1 := \mathbf{H}(\widehat{\mathrm{curl}}; \widehat{\Omega}), \quad \widehat{\mathbb{X}}^2 := L^2(\widehat{\Omega}).$$

Here $\widehat{\mathrm{curl}}$ is the two-dimensional scalar curl operator,

$$\widehat{\mathrm{curl}}(\mathbf{f}) := \partial_{\hat{x}_1} f_2 - \partial_{\hat{x}_2} f_1,$$

for a vector field $\mathbf{f} := (f_1, f_2)$, and $\mathbf{H}(\widehat{\mathrm{curl}}; \widehat{\Omega})$ denotes the space of functions in $\mathbf{L}^2(\widehat{\Omega})$ such that their $\widehat{\mathrm{curl}}$ belongs to $L^2(\widehat{\Omega})$. We have $\widehat{\mathrm{curl}}(\widehat{\nabla} f) = 0$ for any $f \in H^1(\widehat{\Omega})$. In addition, since the domain $\widehat{\Omega}$ is simply connected, we also know that $\mathrm{Im}(\widehat{\nabla}) = \mathrm{Ker}(\widehat{\mathrm{curl}})$, i.e., the following sequence is exact:

$$\mathbb{R} \longrightarrow \widehat{\mathbb{X}}^0 \xrightarrow{\widehat{\nabla}} \widehat{\mathbb{X}}^1 \xrightarrow{\widehat{\mathrm{curl}}} \widehat{\mathbb{X}}^2 \longrightarrow 0. \tag{28}$$

For a proper discretization of continuous problems involving bivariate vector fields like those arising in electromagnetics, it is necessary to construct finite dimensional spaces $\widehat{\mathbb{X}}^j_h \subset \widehat{\mathbb{X}}^j$, $j = 0, 1, 2$ maintaining the same relationships of the continuous spaces given in (28). We are going to construct such finite dimensional spaces by using tensor-product Tchebycheffian spline spaces.

Let $\mathbb{S}^{\mathbf{r}_1,\mathbf{r}_2}_{p_1,p_2}$ denote a bivariate Tchebycheffian spline space defined as (to avoid a too heavy notation, we omit the explicit dependence on w_l, Δ_l, $l = 1, 2$):

$$\mathbb{S}^{\mathbf{r}_1,\mathbf{r}_2}_{p_1,p_2} := \mathbb{S}^{\mathbf{r}_1}_{p_1}(\Delta_1, w_1) \otimes \mathbb{S}^{\mathbf{r}_2}_{p_2}(\Delta_2, w_2). \tag{29}$$

Then, the bivariate Tchebycheffian spline spaces relevant for the discrete de Rham complex are defined as:

$$\begin{aligned}
\widehat{\mathbb{X}}^0_h &:= \mathbb{S}^{\mathbf{r}_1,\mathbf{r}_2}_{p_1,p_2}, \\
\widehat{\mathbb{X}}^1_h &:= \mathbb{S}^{\mathbf{r}_1-\mathbf{1},\mathbf{r}_2}_{p_1-1,p_2} \times \mathbb{S}^{\mathbf{r}_1,\mathbf{r}_2-\mathbf{1}}_{p_1,p_2-1}, \\
\widehat{\mathbb{X}}^2_h &:= \mathbb{S}^{\mathbf{r}_1-\mathbf{1},\mathbf{r}_2-\mathbf{1}}_{p_1-1,p_2-1}.
\end{aligned}$$

We recall that $p_l \geq 1$ and $\mathbf{r}_l \geq \mathbf{0}$, so that the elements of $\widehat{\mathbb{X}}^0_h$ are at least continuous and the spaces $\widehat{\mathbb{X}}^1_h$ and $\widehat{\mathbb{X}}^2_h$ are well defined. In a complete analogy with the polynomial case [5, Section 5.2], we have

$$\widehat{\nabla}(\widehat{\mathbb{X}}^0_h) \subset (\widehat{\mathbb{X}}^1_h), \quad \widehat{\mathrm{curl}}(\widehat{\mathbb{X}}^1_h) \subset (\widehat{\mathbb{X}}^2_h),$$

and from the surjectivity of (15) we conclude that the spaces $\widehat{\mathbb{X}}^j_h$, $j = 0, 1, 2$ form the following exact sequence, which is a discrete version of (28):

$$\mathbb{R} \longrightarrow \widehat{\mathbb{X}}^0_h \xrightarrow{\widehat{\nabla}} \widehat{\mathbb{X}}^1_h \xrightarrow{\widehat{\mathrm{curl}}} \widehat{\mathbb{X}}^2_h \longrightarrow 0. \tag{30}$$

Now, aiming to connect the continuous and the discrete exact sequences (28) and (30), we consider the following projectors:

$$\begin{aligned}
\widehat{\Pi}^0 &:= \widehat{\Pi}^{w_1}_{p_1} \otimes \widehat{\Pi}^{w_2}_{p_2}, \\
\widehat{\Pi}^1 &:= \left(\widehat{\Pi}^{c,w_1}_{p_1-1} \otimes \widehat{\Pi}^{w_2}_{p_2}\right) \times \left(\widehat{\Pi}^{w_1}_{p_1} \otimes \widehat{\Pi}^{c,w_2}_{p_2-1}\right), \\
\widehat{\Pi}^2 &:= \widehat{\Pi}^{c,w_1}_{p_1-1} \otimes \widehat{\Pi}^{c,w_2}_{p_2-1}.
\end{aligned} \tag{31}$$

Since the involved univariate operators are projectors on the corresponding spline spaces (see Section 3.1), we have

$$\begin{aligned}
&\widehat{\Pi}^j f_h = f_h, \quad \forall f_h \in \widehat{\mathbb{X}}^j_h, \quad j = 0, 2, \\
&\widehat{\Pi}^1 \mathbf{f}_h = \mathbf{f}_h, \quad \forall \mathbf{f}_h \in \widehat{\mathbb{X}}^1_h.
\end{aligned} \tag{32}$$

Moreover, the stability results of the involved one-dimensional projectors (see Propositions 4 and 6) immediately give

$$\begin{aligned}
&\|\widehat{\Pi}^0 f\|_{L^2(Q_{\boldsymbol{\ell}})} \leq C \|f\|_{L^2(\widetilde{Q}_{\boldsymbol{\ell}})}, \\
&\|\widehat{\Pi}^1 \mathbf{f}\|_{\mathbf{L}^2(Q_{\boldsymbol{\ell}})} \leq C \|\mathbf{f}\|_{\mathbf{L}^2(\widetilde{Q}_{\boldsymbol{\ell}})}, \\
&\|\widehat{\Pi}^2 f\|_{L^2(Q_{\boldsymbol{\ell}})} \leq C \|f\|_{L^2(\widetilde{Q}_{\boldsymbol{\ell}})},
\end{aligned} \tag{33}$$

where for $\xi_{\ell_l} < \xi_{\ell_l+1}$, $l = 1, 2$,

$$Q_{\boldsymbol{\ell}} := [\xi_{\ell_1}, \xi_{\ell_1+1}] \times [\xi_{\ell_2}, \xi_{\ell_2+1}], \quad \widetilde{Q}_{\boldsymbol{\ell}} := [\xi_{\ell_1-p_1}, \xi_{\ell_1+p_1+1}] \times [\xi_{\ell_2-p_2}, \xi_{\ell_2+p_2+1}].$$

Finally, with the same arguments as in [5, Lemma 5.5], we get

$$\begin{aligned}
&\widehat{\nabla}(\widehat{\Pi}^0 f) = \widehat{\Pi}^1(\widehat{\nabla} f), \qquad \forall f \in \widehat{\mathbb{X}}^0, \\
&\widehat{\mathrm{curl}}(\widehat{\Pi}^1 \mathbf{f}) = \widehat{\Pi}^2(\widehat{\mathrm{curl}}(\mathbf{f})), \quad \forall \mathbf{f} \in \widehat{\mathbb{X}}^1.
\end{aligned} \tag{34}$$

Properties (31)–(34) ensure that, together with the projectors, the considered continuous and discrete spaces form a commuting de Rham diagram and we have the following result.

Proposition 8. *The following commuting de Rham diagram holds:*

$$\begin{array}{ccccccccc}
\mathbb{R} & \longrightarrow & \widehat{\mathbb{X}}^0 & \xrightarrow{\widehat{\nabla}} & \widehat{\mathbb{X}}^1 & \xrightarrow{\widehat{\mathrm{curl}}} & \widehat{\mathbb{X}}^2 & \longrightarrow & 0 \\
 & & \downarrow{\scriptstyle \widehat{\Pi}^0} & & \downarrow{\scriptstyle \widehat{\Pi}^1} & & \downarrow{\scriptstyle \widehat{\Pi}^2} & & \\
\mathbb{R} & \longrightarrow & \widehat{\mathbb{X}}^0_h & \xrightarrow{\widehat{\nabla}} & \widehat{\mathbb{X}}^1_h & \xrightarrow{\widehat{\mathrm{curl}}} & \widehat{\mathbb{X}}^2_h & \longrightarrow & 0
\end{array} \tag{35}$$

The above spaces do not have boundary conditions. Completely similar constructions can be provided for spaces incorporating homogeneous boundary conditions on (parts of) $\partial\widehat{\Omega}$ as outlined at the end of Section 3.2.

In the two-dimensional case, the following differential operator is also of interest:

$$\widehat{\mathbf{rot}}(f) := (\partial_{\widehat{x}_2} f, -\partial_{\widehat{x}_1} f).$$

Setting $\widehat{\mathbb{X}}^{0,*} := H^1(\widehat{\Omega})$, $\widehat{\mathbb{X}}^{1,*} := \mathbf{H}(\widehat{\mathrm{div}};\widehat{\Omega})$, and $\widehat{\mathbb{X}}^{2,*} := L^2(\widehat{\Omega})$, we have the exact sequence

$$\mathbb{R} \longrightarrow \widehat{\mathbb{X}}^{0,*} \xrightarrow{\widehat{\mathbf{rot}}} \widehat{\mathbb{X}}^{1,*} \xrightarrow{\widehat{\mathrm{div}}} \widehat{\mathbb{X}}^{2,*} \longrightarrow 0. \tag{36}$$

To get a discrete version of (36), we define $\widehat{\mathbb{X}}_h^{0,*} := \widehat{\mathbb{X}}_h^0$, $\widehat{\mathbb{X}}_h^{2,*} := \widehat{\mathbb{X}}_h^2$, and

$$\widehat{\mathbb{X}}_h^{1,*} := \mathbb{S}^{\mathbf{r}_1,\mathbf{r}_2-\mathbf{1}}_{p_1,p_2-1} \times \mathbb{S}^{\mathbf{r}_1-\mathbf{1},\mathbf{r}_2}_{p_1-1,p_2},$$

which leads to the exact sequence

$$\mathbb{R} \longrightarrow \widehat{\mathbb{X}}_h^{0,*} \xrightarrow{\widehat{\mathbf{rot}}} \widehat{\mathbb{X}}_h^{1,*} \xrightarrow{\widehat{\mathrm{div}}} \widehat{\mathbb{X}}_h^{2,*} \longrightarrow 0. \tag{37}$$

By defining the corresponding projectors in a complete analogy with (31), the exact sequences (36) and (37) can be connected to form a commuting de Rham diagram analogous to (35). Also here homogeneous boundary conditions can be easily incorporated.

Note that the superscript $*$ in (36)–(37) is merely a label that distinguishes the two two-dimensional complexes and does not denote the Hodge star operator, $\star$, for differential forms. Nevertheless, the spaces of vector-fields in the complexes (28) and (36) can be thought of as two choices for discretizing differential forms related by the Hodge star operator [28]. This is also reflected in the corresponding pullbacks ι^1 and $\iota^{1,*}$ introduced later in Section 4.3.

Consider, for example, a smooth differential 1-form u in two dimensions. While at the continuous level one can freely pass between the vector proxies related to u and $\star u$, this is no longer true at the discrete level. In the framework of finite element exterior calculus, discrete Hodge star operators can be used to identify the degrees of freedom of one complex with those of the other; see [29] for the polynomial case and [30] for an analysis of discrete Hodge-star operators in the spline setting, as well as [31] for the general theory of discrete Hodge operators.

Since our Tchebycheffian spline spaces have a similar structure to the polynomial spline spaces, the discrete Hodge star operators of [30] can likely be generalized to the present setting. Continuing with the two-dimensional case and following [30], we consider the following diagram where the top row is the discrete complex from (30) with zero boundary conditions, and the bottom row is the complex from (37) (note that we assume that every entry in $\mathbf{r}_1$ and $\mathbf{r}_2$ is at least 1):

$$\begin{array}{ccccc}
\widehat{\mathbb{X}}^0_{h,0} := \mathbb{S}^{\mathbf{r}_1,\mathbf{r}_2}_{p_1,p_2} \cap \widehat{\mathbb{X}}^0_0 & \longrightarrow & \widehat{\mathbb{X}}^1_{h,0} := \mathbb{S}^{\mathbf{r}_1-\mathbf{1},\mathbf{r}_2}_{p_1-1,p_2} \times \mathbb{S}^{\mathbf{r}_1,\mathbf{r}_2-\mathbf{1}}_{p_1,p_2-1} \cap \widehat{\mathbb{X}}^1_0 & \longrightarrow & \widehat{\mathbb{X}}^2_{h,0} := \mathbb{S}^{\mathbf{r}_1-\mathbf{1},\mathbf{r}_2-\mathbf{1}}_{p_1-1,p_2-1} \cap \widehat{\mathbb{X}}^2_0 \\
\downarrow \star_h^0 & & \downarrow \star_h^1 & & \downarrow \star_h^2 \\
\widehat{\mathbb{X}}^{2,*}_h := \mathbb{S}^{\mathbf{r}_1-\mathbf{2},\mathbf{r}_2-\mathbf{2}}_{p_1-2,p_2-2} & \longleftarrow & \widehat{\mathbb{X}}^{1,*}_h := \mathbb{S}^{\mathbf{r}_1-\mathbf{1},\mathbf{r}_2-\mathbf{2}}_{p_1-1,p_2-2} \times \mathbb{S}^{\mathbf{r}_1-\mathbf{2},\mathbf{r}_2-\mathbf{1}}_{p_1-2,p_2-1} & \longleftarrow & \widehat{\mathbb{X}}^{0,*}_h := \mathbb{S}^{\mathbf{r}_1-\mathbf{1},\mathbf{r}_2-\mathbf{1}}_{p_1-1,p_2-1}
\end{array},$$

where $\widehat{\mathbb{X}}^k_0$ denote the relevant continuous spaces with homogeneous boundary conditions on the appropriate traces [1]. The discrete Hodge star operator $\star_h^k$ mapping the degrees of freedom of $u_h \in \widehat{\mathbb{X}}^k_{h,0}$ to those of $\star_h^k u_h \in \widehat{\mathbb{X}}^{2-k,*}_h$ can be defined as $(\mathbf{K}^k)^{-1}\mathbf{M}^k$, where $\mathbf{M}^k$ is the mass matrix for $\widehat{\mathbb{X}}^k_{h,0}$ and $\mathbf{K}^k$ is the L^2-pairing matrix between $\widehat{\mathbb{X}}^k_{h,0}$ and $\widehat{\mathbb{X}}^{2-k,*}_h$ [30]. The stability of the latter pairing has been established for polynomial B-splines in [32], but the arguments can likely be extended to the Tchebycheffian setting given the structural similarities between the polynomial and Tchebycheffian settings.

4.2. Three-dimensional case

We now address the construction of a discrete de Rham complex in three dimensions. We follow the same approach and the same notation as in the bivariate case. We just outline the construction, omitting the details that are completely analogous to the bivariate case.

For $\widehat{\Omega} := (0,1)^3$, we set

$$\widehat{\mathbb{X}}^0 := H^1(\widehat{\Omega}), \quad \widehat{\mathbb{X}}^1 := \mathbf{H}(\widehat{\mathbf{curl}};\widehat{\Omega}), \quad \widehat{\mathbb{X}}^2 := \mathbf{H}(\widehat{\mathrm{div}};\widehat{\Omega}), \quad \widehat{\mathbb{X}}^3 := L^2(\widehat{\Omega}),$$

and we consider the exact sequence

$$\mathbb{R} \longrightarrow \widehat{\mathbb{X}}^0 \xrightarrow{\widehat{\nabla}} \widehat{\mathbb{X}}^1 \xrightarrow{\widehat{\mathbf{curl}}} \widehat{\mathbb{X}}^2 \xrightarrow{\widehat{\mathrm{div}}} \widehat{\mathbb{X}}^3 \longrightarrow 0.$$

Let $\mathbb{S}^{\mathbf{r}_1,\mathbf{r}_2,\mathbf{r}_3}_{p_1,p_2,p_3}$ denote a trivariate Tchebycheffian spline space defined as:

$$\mathbb{S}^{\mathbf{r}_1,\mathbf{r}_2,\mathbf{r}_3}_{p_1,p_2,p_3} := \mathbb{S}^{\mathbf{r}_1}_{p_1}(\Delta_1,w_1) \otimes \mathbb{S}^{\mathbf{r}_2}_{p_2}(\Delta_2,w_2) \otimes \mathbb{S}^{\mathbf{r}_3}_{p_3}(\Delta_3,w_3). \tag{38}$$

Then, the trivariate Tchebycheffian spline spaces relevant for the discrete de Rham complex are defined as:

$$\begin{aligned}
\widehat{\mathbb{X}}^0_h &:= \mathbb{S}^{\mathbf{r}_1,\mathbf{r}_2,\mathbf{r}_3}_{p_1,p_2,p_3}, \\
\widehat{\mathbb{X}}^1_h &:= \mathbb{S}^{\mathbf{r}_1-\mathbf{1},\mathbf{r}_2,\mathbf{r}_3}_{p_1-1,p_2,p_3} \times \mathbb{S}^{\mathbf{r}_1,\mathbf{r}_2-\mathbf{1},\mathbf{r}_3}_{p_1,p_2-1,p_3} \times \mathbb{S}^{\mathbf{r}_1,\mathbf{r}_2,\mathbf{r}_3-\mathbf{1}}_{p_1,p_2,p_3-1}, \\
\widehat{\mathbb{X}}^2_h &:= \mathbb{S}^{\mathbf{r}_1,\mathbf{r}_2-\mathbf{1},\mathbf{r}_3-\mathbf{1}}_{p_1,p_2-1,p_3-1} \times \mathbb{S}^{\mathbf{r}_1-\mathbf{1},\mathbf{r}_2,\mathbf{r}_3-\mathbf{1}}_{p_1-1,p_2,p_3-1} \times \mathbb{S}^{\mathbf{r}_1-\mathbf{1},\mathbf{r}_2-\mathbf{1},\mathbf{r}_3}_{p_1-1,p_2-1,p_3},
\end{aligned}$$

$$\widehat{\mathbb{X}}_h^3 := \mathbb{S}^{\mathbf{r}_1-\mathbf{1},\mathbf{r}_2-\mathbf{1},\mathbf{r}_3-\mathbf{1}}_{p_1-1,p_2-1,p_3-1}.$$

They form the exact sequence

$$\mathbb{R} \longrightarrow \widehat{\mathbb{X}}_h^0 \xrightarrow{\widehat{\nabla}} \widehat{\mathbb{X}}_h^1 \xrightarrow{\widehat{\mathbf{curl}}} \widehat{\mathbb{X}}_h^2 \xrightarrow{\widehat{\mathrm{div}}} \widehat{\mathbb{X}}_h^3 \longrightarrow 0. \tag{39}$$

The connection between the continuous and the discrete sequences is obtained by means of the following projectors:

$$\begin{aligned}
\widehat{\Pi}^0 &:= \widehat{\Pi}^{\mathcal{W}_1}_{p_1} \otimes \widehat{\Pi}^{\mathcal{W}_2}_{p_2} \otimes \widehat{\Pi}^{\mathcal{W}_3}_{p_3},\\
\widehat{\Pi}^1 &:= \big(\widehat{\Pi}^{c,\mathcal{W}_1}_{p_1-1} \otimes \widehat{\Pi}^{\mathcal{W}_2}_{p_2} \otimes \widehat{\Pi}^{\mathcal{W}_3}_{p_3}\big) \times \big(\widehat{\Pi}^{\mathcal{W}_1}_{p_1} \otimes \widehat{\Pi}^{c,\mathcal{W}_2}_{p_2-1} \otimes \widehat{\Pi}^{\mathcal{W}_3}_{p_3}\big) \times \big(\widehat{\Pi}^{\mathcal{W}_1}_{p_1} \otimes \widehat{\Pi}^{\mathcal{W}_2}_{p_2} \otimes \widehat{\Pi}^{c,\mathcal{W}_3}_{p_3-1}\big),\\
\widehat{\Pi}^2 &:= \big(\widehat{\Pi}^{\mathcal{W}_1}_{p_1} \otimes \widehat{\Pi}^{c,\mathcal{W}_2}_{p_2-1} \otimes \widehat{\Pi}^{c,\mathcal{W}_3}_{p_3-1}\big) \times \big(\widehat{\Pi}^{c,\mathcal{W}_1}_{p_1-1} \otimes \widehat{\Pi}^{\mathcal{W}_2}_{p_2} \otimes \widehat{\Pi}^{c,\mathcal{W}_3}_{p_3-1}\big) \times \big(\widehat{\Pi}^{c,\mathcal{W}_1}_{p_1-1} \otimes \widehat{\Pi}^{c,\mathcal{W}_2}_{p_2-1} \otimes \widehat{\Pi}^{\mathcal{W}_3}_{p_3}\big),\\
\widehat{\Pi}^3 &:= \widehat{\Pi}^{c,\mathcal{W}_1}_{p_1-1} \otimes \widehat{\Pi}^{c,\mathcal{W}_2}_{p_2-1} \otimes \widehat{\Pi}^{c,\mathcal{W}_3}_{p_3-1}.
\end{aligned}$$

From the properties of the involved univariate projectors it is easy to see that we get the analog of (31)–(34) for the trivariate case. Therefore, together with the projectors, the considered continuous and discrete spaces form a discrete de Rham diagram, as stated in the following proposition.

Proposition 9. *The following commuting de Rham diagram holds:*

$$\begin{array}{ccccccccccc}
\mathbb{R} & \longrightarrow & \widehat{\mathbb{X}}^0 & \xrightarrow{\widehat{\nabla}} & \widehat{\mathbb{X}}^1 & \xrightarrow{\widehat{\mathbf{curl}}} & \widehat{\mathbb{X}}^2 & \xrightarrow{\widehat{\mathrm{div}}} & \widehat{\mathbb{X}}^3 & \longrightarrow & 0\\
 & & \downarrow{\scriptstyle \widehat{\Pi}^0} & & \downarrow{\scriptstyle \widehat{\Pi}^1} & & \downarrow{\scriptstyle \widehat{\Pi}^2} & & \downarrow{\scriptstyle \widehat{\Pi}^3} & & \\
\mathbb{R} & \longrightarrow & \widehat{\mathbb{X}}_h^0 & \xrightarrow{\widehat{\nabla}} & \widehat{\mathbb{X}}_h^1 & \xrightarrow{\widehat{\mathbf{curl}}} & \widehat{\mathbb{X}}_h^2 & \xrightarrow{\widehat{\mathrm{div}}} & \widehat{\mathbb{X}}_h^3 & \longrightarrow & 0
\end{array}. \tag{40}$$

4.3. Mapped domains

We now briefly discuss how the above constructions can be extended to physical domains Ω that are images of the parametric domain $\widehat{\Omega} \subset \mathbb{R}^d$, $d = 2, 3$, through a sufficiently regular and invertible geometric map $\mathbf{F} : \widehat{\Omega} \to \Omega$. Given spaces $\widehat{\mathbb{X}}_h^j$, $j = 0, \dots, d$ that form a discrete de Rham complex on $\widehat{\Omega}$, we can define the corresponding physical spaces on Ω as follows:

$$\mathbb{X}_h^j := \left\{ v_h : \iota^j(v_h) \in \widehat{\mathbb{X}}_h^j \right\} \subset \mathbb{X}^j, \tag{41}$$

where ι^j are pullback operators and $\mathbb{X}^j$ are the continuous spaces that form the de Rham complex on Ω; both are defined as below, with $D\mathbf{F}$ denoting the Jacobian matrix of the geometric map $\mathbf{F}$.

- Two-dimensional complex (30):

$$\begin{aligned}
\mathbb{X}^0 &:= H^1(\Omega), & \iota^0(v) &:= v \circ \mathbf{F},\\
\mathbb{X}^1 &:= \mathbf{H}(\mathrm{curl}; \Omega), & \iota^1(\mathbf{v}) &:= (D\mathbf{F})^{\mathrm{T}}(\mathbf{v} \circ \mathbf{F}),\\
\mathbb{X}^2 &:= L^2(\Omega), & \iota^2(v) &:= \det(D\mathbf{F})(v \circ \mathbf{F}).
\end{aligned}$$

- Two-dimensional complex (37):

$$\begin{aligned}
\mathbb{X}^0 &:= H^1(\Omega), & \iota^0(v) &:= v \circ \mathbf{F},\\
\mathbb{X}^{1,*} &:= \mathbf{H}(\mathrm{div}; \Omega), & \iota^{1,*}(\mathbf{v}) &:= \det(D\mathbf{F})(D\mathbf{F})^{-1}(\mathbf{v} \circ \mathbf{F}),\\
\mathbb{X}^2 &:= L^2(\Omega), & \iota^2(v) &:= \det(D\mathbf{F})(v \circ \mathbf{F}).
\end{aligned}$$

- Three-dimensional complex (39):

$$\begin{aligned}
\mathbb{X}^0 &:= H^1(\Omega), & \iota^0(v) &:= v \circ \mathbf{F},\\
\mathbb{X}^1 &:= \mathbf{H}(\mathbf{curl}; \Omega), & \iota^1(\mathbf{v}) &:= (D\mathbf{F})^{\mathrm{T}}(\mathbf{v} \circ \mathbf{F}),\\
\mathbb{X}^2 &:= \mathbf{H}(\mathrm{div}; \Omega), & \iota^2(\mathbf{v}) &:= \det(D\mathbf{F})(D\mathbf{F})^{-1}(\mathbf{v} \circ \mathbf{F}),\\
\mathbb{X}^3 &:= L^2(\Omega), & \iota^3(v) &:= \det(D\mathbf{F})(v \circ \mathbf{F}).
\end{aligned}$$

The corresponding spaces $\mathbb{X}_h^j$, $j = 0, \dots, d$ form a discrete de Rham complex on Ω and the following diagram commutes; see [3] for details:

$$\begin{array}{ccccccccc}
\mathbb{R} & \longrightarrow & \mathbb{X}_h^0 & \longrightarrow & \cdots & \longrightarrow & \mathbb{X}_h^d & \longrightarrow & 0\\
 & & \downarrow{\scriptstyle \iota^0} & & & & \downarrow{\scriptstyle \iota^d} & & \\
\mathbb{R} & \longrightarrow & \widehat{\mathbb{X}}_h^0 & \longrightarrow & \cdots & \longrightarrow & \widehat{\mathbb{X}}_h^d & \longrightarrow & 0
\end{array}. \tag{42}$$

5. Numerical results

In this section we present numerical results for different problems solved with the isogeometric discretizations introduced in Section 4. We consider three different problems: the Hodge–Laplace problem in Section 5.1, the Maxwell eigenvalue problem in Section 5.2, and the Oseen problem in Section 5.3. We used `Mantis.jl` for all numerical simulations [22], which is an open-source software for performing isogeometric structure-preserving simulations written in the Julia programming language.

5.1. Convergence results on a mapped geometry

Consider a domain $\Omega = (0,1)^2$, which is parameterized by mapping the parametric domain $(0,1)^2$ to itself via the following Colella map $\mathbf{F}$:

$$(x_1, x_2) = \mathbf{F}(\hat{x}_1, \hat{x}_2) = \Big(\hat{x}_1 + \frac{1}{20}\sin(\pi(2\hat{x}_1 - 1))\sin(\pi(2\hat{x}_2 - 1)),\ \hat{x}_2 + \frac{1}{20}\sin(\pi(2\hat{x}_1 - 1))\sin(\pi(2\hat{x}_2 - 1))\Big).$$

On this domain, with $\mathbf{n}$ denoting the outward normal vector, we consider the following spaces with homogeneous boundary conditions:

$$\mathbb{X}^0_{h,0} := \big\{v_h \in \mathbb{X}^0_h : v_h = 0 \text{ on } \partial\Omega\big\},$$
$$\mathbb{X}^1_{h,\|,0} := \big\{\mathbf{v}_h \in \mathbb{X}^1_h : \mathbf{v}_h \times \mathbf{n} = 0 \text{ on } \partial\Omega\big\}.$$

We will use the above spaces to solve the three (mixed) weak forms of the Hodge–Laplace problem in two spatial dimensions, i.e., two scalar problems and one vector-valued problem. The exact solutions to the continuous problems are chosen as

$$u^0 = \frac{x_1(1-x_1)x_2(1-x_2)}{1+x_1+x_2},$$
$$\mathbf{u}^1 = \left(\frac{x_1(1-x_1)x_2(1-x_2)}{1+x_1+x_2}, \frac{x_1(1-x_1)x_2(1-x_2)}{1+x_1+x_2}\right),$$
$$u^2 = \frac{x_1(1-x_1)x_2(1-x_2)}{1+x_1+x_2},$$

and the corresponding right-hand sides are chosen as $f^0 = -\Delta u^0$, $\mathbf{f}^1 = -\Delta \mathbf{u}^1$, and $f^2 = -\Delta u^2$, respectively. The discretized Hodge–Laplace problems can be stated as follows:

- HL^0: find $u_h \in \mathbb{X}^0_{h,0}$ such that

$$(\nabla u_h, \nabla v_h) = (f^0, v_h), \quad \forall v_h \in \mathbb{X}^0_{h,0};$$

- HL^1: find $(\sigma_h, \mathbf{u}_h) \in \mathbb{X}^0_h \times \mathbb{X}^1_{h,\|,0}$ such that

$$(\sigma_h, \tau_h) + (\nabla\tau_h, \mathbf{u}_h) = 0, \qquad \forall \tau_h \in \mathbb{X}^0_h,$$
$$-(\nabla\sigma_h, \mathbf{v}_h) + (\mathrm{curl}(\mathbf{u}_h), \mathrm{curl}(\mathbf{v}_h)) = (\mathbf{f}^1, \mathbf{v}_h), \quad \forall \mathbf{v}_h \in \mathbb{X}^1_{h,\|,0};$$

- HL^2: find $(\boldsymbol{\sigma}_h, u_h) \in \mathbb{X}^1_h \times \mathbb{X}^2_h$ such that

$$(\boldsymbol{\sigma}_h, \boldsymbol{\tau}_h) - (\mathrm{curl}(\boldsymbol{\tau}_h), u_h) = 0, \qquad \forall \boldsymbol{\tau}_h \in \mathbb{X}^1_h,$$
$$(\mathrm{curl}(\boldsymbol{\sigma}_h), v_h) = (f^2, v_h), \quad \forall v_h \in \mathbb{X}^2_h.$$

Note that homogeneous natural boundary conditions have been imposed in HL^1 and HL^2, respectively, for the normal trace of $\mathbf{u}_h$ and the trace of u_h.

We solve the above problems with maximally smooth (tensor-product) Tchebycheffian splines that fit in a de Rham complex as in (42) obtained from (35). We do so such that the bi-degree in $\mathbb{X}^0_h$ is (p,p), with $p \in \{2,3,4\}$. We use generalized exponential spaces ($\mathbb{P}^{(\alpha,-\alpha)}_p$ as in (9)) and generalized trigonometric spaces ($\mathbb{P}^{(i\beta,-i\beta)}_p$ as in (10)) whose parameters are chosen to be $\alpha = 10$ and $\beta = 2\pi$, respectively. Note that for $p = 2$, the spaces do not contain linear polynomials and so the (Tchebycheffian) Greville abscissae in (16) are not well defined; however, this does not affect optimal convergence of the corresponding approximations. We also compare these spaces with standard polynomial spaces of the same degree p. All parametric domain partitions are uniform, with the coarsest mesh employing 4×4 elements. The L^2 errors for each relevant object are shown in Fig. 1 for HL^0, in Fig. 2 for HL^1, and in Fig. 3 for HL^2; all errors are plotted against the square-root of the number of degrees of freedom for the corresponding space. As can be seen, all unknowns in $\mathbb{X}^0_h$, $\mathbb{X}^1_h$, and $\mathbb{X}^2_h$ converge to the exact solutions with the optimal rates of $p+1$, p, and p with respect to L^2 norms, respectively.

5.2. Maxwell eigenvalue problem

In this section we consider the Maxwell eigenvalue problem on a domain $\Omega = (0,a) \times (0,b) \subset \mathbb{R}^2$ with perfectly conducting boundary conditions: find $(\lambda, \mathbf{u}) \in \mathbb{R} \times \mathbb{X}^1_{\|,0}$ such that

$$(\mathrm{curl}(\mathbf{u}), \mathrm{curl}(\mathbf{v})) = \lambda(\mathbf{u}, \mathbf{v}), \quad \forall \mathbf{v} \in \mathbb{X}^1_{\|,0},$$

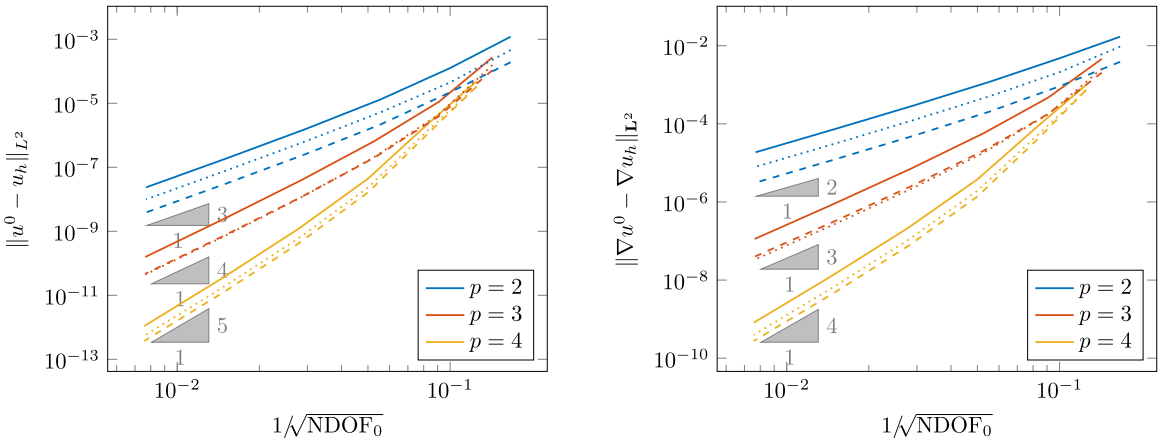


Fig. 1. Error convergence results for HL^0: the solid lines correspond to generalized exponential splines, the dashed lines correspond to generalized trigonometric splines, and the dotted lines correspond to polynomial splines. The left column shows the errors for u_h, the right column shows the errors for ∇u_h.

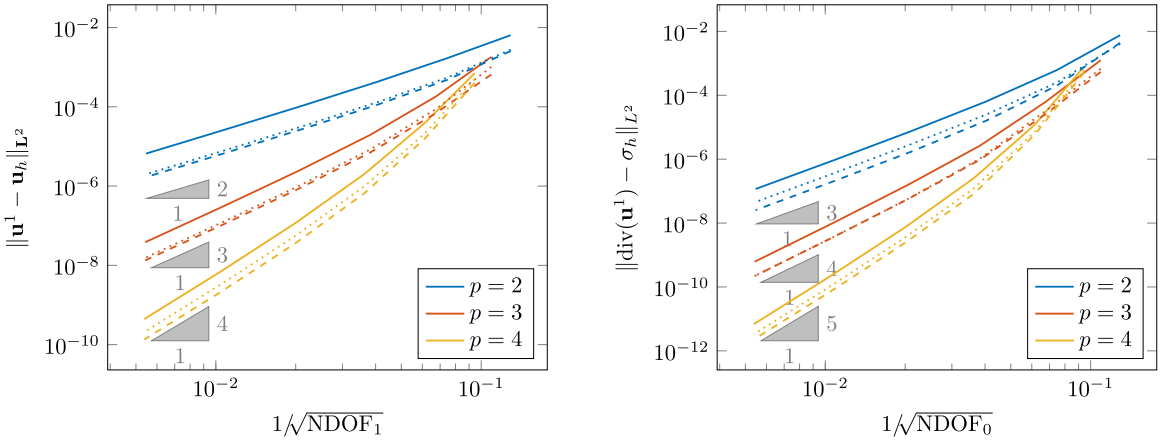


Fig. 2. Error convergence results for HL^1: the solid lines correspond to generalized exponential splines, the dashed lines correspond to generalized trigonometric splines, and the dotted lines correspond to polynomial splines. The left column shows the errors for $\mathbf{u}_h$, the right column shows the errors for σ_h.

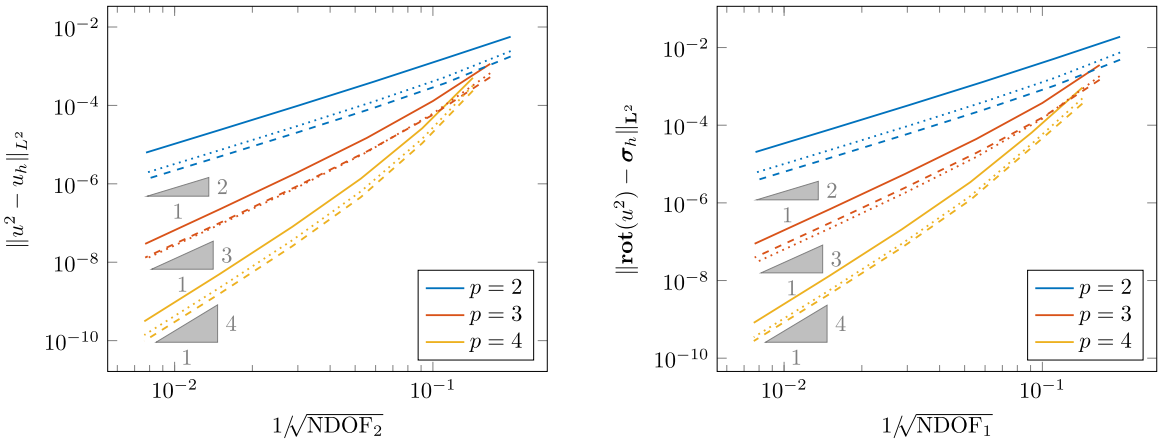


Fig. 3. Error convergence results for HL^2: the solid lines correspond to generalized exponential splines, the dashed lines correspond to generalized trigonometric splines, and the dotted lines correspond to polynomial splines. The left column shows the errors for u_h, the right column shows the errors for $\boldsymbol{\sigma}_h$.

Table 1
First eight exact and computed eigenvalues for the Maxwell eigenvalue problem on $\Omega = (0,\pi)^2$. The eigenvalues computed with all three spline spaces are very close to the exact ones, and almost identical to each other.

Mode	Exact	$\mathbb{P}_3$	$\mathbb{P}_3^{(2\pi i,-2\pi i)}$	$\mathbb{P}_3^{(10,-10)}$
(1, 0)	01.0000000000000	1.0000000019300	1.0000000019300	1.0000000019300
(0, 1)	01.0000000000000	1.0000000019300	1.0000000019300	1.0000000019300
(1, 1)	02.0000000000000	2.0000000038601	2.0000000038600	2.0000000038600
(2, 0)	04.0000000000000	4.0000005214206	4.0000005214206	4.0000005214206
(0, 2)	04.0000000000000	4.0000005214206	4.0000005214206	4.0000005214206
(2, 1)	05.0000000000000	5.0000005233506	5.0000005233506	5.0000005233506
(1, 2)	05.0000000000000	5.0000005233507	5.0000005233506	5.0000005233506
(2, 2)	08.0000000000000	8.0000010428413	8.0000010428413	8.0000010428413

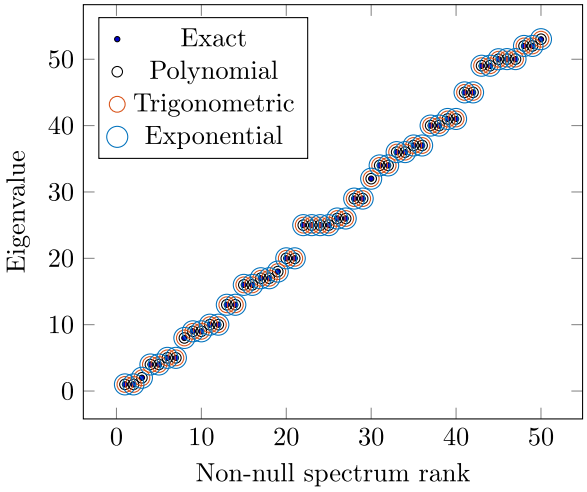


Fig. 4. We compare the first 50 analytical and computed eigenvalues for the Maxwell eigenvalue problem on $\Omega = (0,\pi)^2$ for maximally smooth bi-cubic polynomial, generalized trigonometric, and generalized exponential spline spaces. No spurious eigenvalues are present in the computed spectra.

where

$$\mathbb{X}^1_{\|,0} := \{\mathbf{v} \in \mathbb{X}^1 \,:\, \mathbf{v}\times\mathbf{n} = 0 \text{ on } \partial\Omega\}.$$

The analytical eigenvalue corresponding to mode (m,n) is equal to $\lambda/\pi^2 = (m/a)^2 + (n/b)^2$ with $(m,n) \in \{0,1,\dots\}^2\backslash\{(0,0)\}$. In the following tests, the domain is parameterized by scaling the parametric domain $(0,1)^2$, and we consider a Galerkin discretization of the problem by searching for the eigenvectors in the discrete space $\mathbb{X}^1_{h,\|,0}$ defined in Section 5.1: find $(\lambda_h, \mathbf{u}_h) \in \mathbb{R}\times\mathbb{X}^1_{h,\|,0}$ such that

$$(\mathrm{curl}(\mathbf{u}_h), \mathrm{curl}(\mathbf{v}_h)) = \lambda_h(\mathbf{u}_h, \mathbf{v}_h), \quad \forall \mathbf{v}_h \in \mathbb{X}^1_{h,\|,0}.$$

5.2.1. Comparison of the spectra obtained with different spline spaces

We take $\Omega = (0,\pi)^2$ (i.e., $a = b = \pi$) and discretize using three types of maximally smooth spline vector fields (polynomial, generalized trigonometric, generalized exponential) from a discrete de Rham complex built for bi-degree $(p_1, p_2) = (3,3)$ and on a uniform 16×16 mesh. The trigonometric parameter in all tests is chosen to be $\beta = 2\pi$ and the exponential parameter is chosen to be $\alpha = 10$. In Table 1 we show the first computed eigenvalues compared against the analytical ones. The first 50 eigenvalues are plotted in Fig. 4, and we see that we get the correct spectrum without any spurious eigenvalues. This behavior is well understood within the general theory of mixed finite element approximation of eigenvalue problems [33]: the appearance of spurious modes is ruled out precisely when the discretization inherits the cohomological structure of the continuous problem. More specifically, this happens when the discrete spaces form an exact subcomplex equipped with bounded commuting projections, so that a discrete compactness property holds. Our Tchebycheffian de Rham complexes (35) satisfy exactly these requirements, which explains the spectrally-correct, spurious-free spectra observed here.

5.2.2. Convergence results for specific eigenvalues

Next, with $\Omega = (0,\pi)\times(0,1)$ (i.e., $a = \pi$, $b = 1$) and starting from a 3×3 uniform mesh and different choices of degrees, we refine the mesh for the same three types of spline spaces (polynomial, generalized trigonometric, generalized exponential) and compute the error in the eigenvalues corresponding to modes $(1,1)$ and $(2,0)$. The convergence results for the errors are shown in Fig. 5, and the

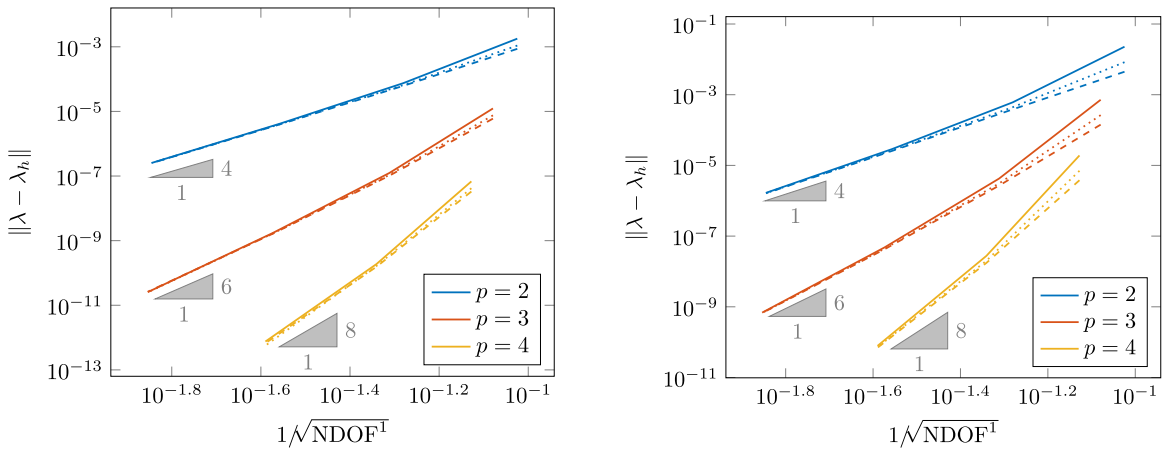


Fig. 5. Error convergence results for the Maxwell eigenvalue problem on $\Omega = (0, \pi) \times (0, 1)$: the solid lines correspond to generalized exponential splines, the dashed lines correspond to generalized trigonometric splines, and the dotted lines correspond to polynomial splines. The left column shows mode $(1, 1)$, the right column shows mode $(2, 0)$.

expected optimal convergence of order $2p$ is observed in all cases. Note that the special choice of the domain size in this test is made to easily distinguish between modes (m, n) (with eigenvalue $m^2 + \pi^2 n^2$) and (n, m) (with eigenvalue $n^2 + \pi^2 m^2$).

Beyond the convergence of individual eigenvalues, the global behavior of the computed spectrum can be characterized through the notion of spectral symbol, which describes the asymptotic spectral distribution of the discretization matrices as the mesh is refined. Symbol-based analysis is a useful tool for studying finite element and isogeometric B-spline discretizations of eigenvalue problems, including the precise description of the so-called optical branches and outliers of the spectrum; see [34] for an exposition and review. The same methodology has recently been employed in the setting of differential forms [35]. Extending the symbol-based analysis to the Tchebycheffian de Rham discretizations proposed here, so as to predict the spectral distribution as a function of the shape parameters of the underlying ECT-spaces, is an interesting direction that we leave for future work. Symbols related to some specific Tchebycheffian spline spaces, with a single shape parameter as in (9) and (10), have already been investigated in [36,37].

5.3. Oseen flow

Given a domain $\Omega \subset \mathbb{R}^2$, consider the following velocity-vorticity-pressure formulation of the Oseen problem with homogeneous tangential (natural) and normal (essential) boundary conditions: for $\mathbf{f} \in \mathbb{X}^{1,*}$, find $(\omega_h, \mathbf{u}_h, p_h, \lambda_h) \in \mathbb{X}^0_h \times \mathbb{X}^{1,*}_{h,0} \times \mathbb{X}^2_h \times \mathfrak{h}^2$ such that

$$\begin{aligned}
(\sigma_h, \omega_h) - (\mathbf{rot}(\sigma_h), \mathbf{u}_h) &= 0, && \forall \sigma_h \in \mathbb{X}^0_h, \\
(\mathbf{v}_h, \mathbf{U} \times \omega_h) - \nu(\mathbf{v}_h, \mathbf{rot}(\omega_h)) + (\nabla \cdot \mathbf{v}_h, p_h) &= (\mathbf{v}_h, \mathbf{f}), && \forall \mathbf{v}_h \in \mathbb{X}^{1,*}_{h,0}, \\
(q_h, \nabla \cdot \mathbf{u}_h) + (q_h, \lambda_h) &= 0, && \forall q_h \in \mathbb{X}^2_h, \\
(\theta_h, p_h) &= 0, && \forall \theta_h \in \mathfrak{h}^2,
\end{aligned}$$

where $\mathfrak{h}^2 \cong \mathbb{R}$ is the one-dimensional space of harmonic 2-forms, ν is the viscosity, $\mathbf{U}$ is a divergence-free advecting velocity field, and $\mathbb{X}^{1,*}_{h,0}$ is the space of vector fields in $\mathbb{X}^{1,*}_h$ with vanishing normal component on the boundary of Ω,

$$\mathbb{X}^{1,*}_{h,0} := \left\{ \mathbf{v}_h \in \mathbb{X}^{1,*}_h \,:\, \mathbf{v}_h \cdot \mathbf{n} = 0 \text{ on } \partial\Omega \right\}.$$

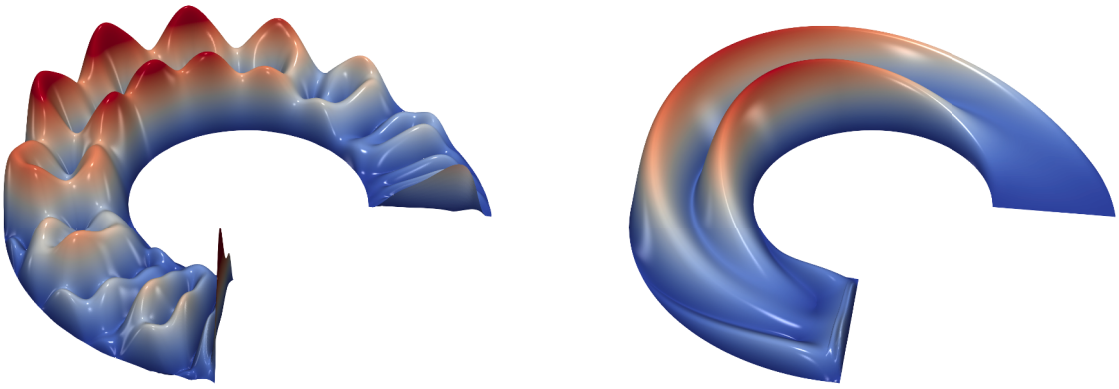
Here $\mathbf{u}_h$ is the unknown velocity field, ω_h is the associated vorticity, p_h is the pressure, and λ_h is a Lagrange multiplier enforcing the compatibility condition for the pressure. While the normal component of the velocity is strongly prescribed, the tangential component is weakly set to zero by the first sub-equation in the weak formulation.

For the numerical tests, we choose Ω as a three-quarters annulus centered at the origin with inner and outer radius equal to 1 and 2, respectively. The domain is parameterized by the following geometric map $\mathbf{F}$:

$$(x_1, x_2) = \mathbf{F}(\hat{x}_1, \hat{x}_2) = \big((\hat{x}_2 + 1)\cos(3\pi\hat{x}_1/2),\ (\hat{x}_2 + 1)\sin(3\pi\hat{x}_1/2)\big).$$

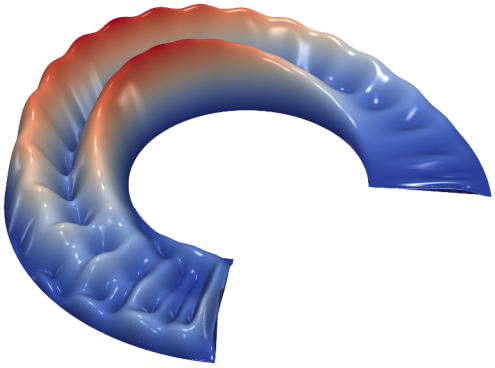
Furthermore, we take $\mathbf{U} = (-\sin(\theta), \cos(\theta))$, $\nu^{-1} = 100$, $\mathbf{f} = (0, x_1 x_2)$, and solve the problem on meshes with 20×5, 40×10, and 80×20 elements.

The numerical results are shown in Fig. 6. We only show the magnitudes of the computed velocity fields for brevity. The left column shows the results obtained by using maximally smooth polynomial splines of bi-degree $(6, 6)$. The right column shows the results obtained using maximally smooth Tchebycheffian splines of bi-degree $(6, 6)$ built as the tensor product of Tchebycheffian splines in $\hat{x}_1$ direction (with exponential parameters $\alpha_1 = -3\pi/2\nu$, $\alpha_2 = -9\pi/4\nu$, $\alpha_3 = -3\pi/\nu$, and with trigonometric parameter $\beta = 3\pi/2$) and polynomial splines in $\hat{x}_2$ direction. We motivate the choice of these parameters as follows.

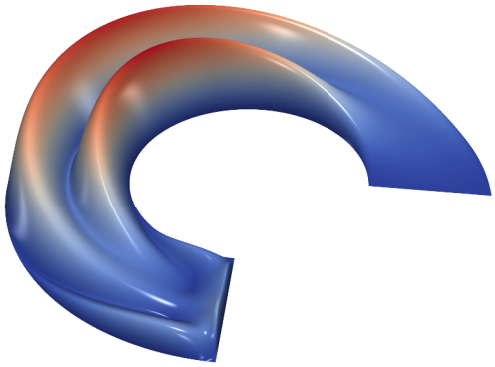


(a) Polynomial; 20×5 elements

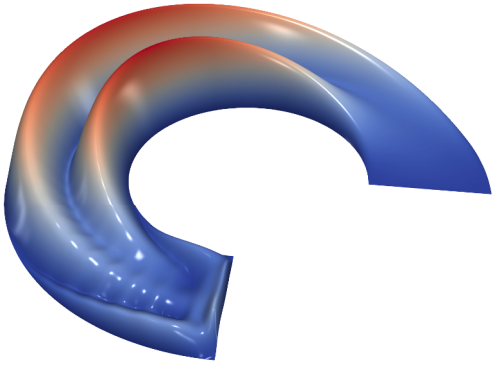
(b) Tchebycheffian; 20×5 elements



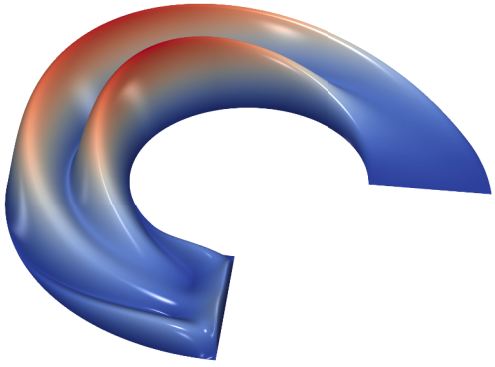
(c) Polynomial; 40×10 elements



(d) Tchebycheffian; 40×10 elements



(e) Polynomial; 80×20 elements



(f) Tchebycheffian; 80×20 elements

Fig. 6. Magnitude of the velocity field for the Oseen flow problem with polynomial splines (left) and Tchebycheffian splines (right), both of bi-degree $(6, 6)$, on meshes with 20×5 (top), 40×10 (middle), and 80×20 (bottom) elements.

- The trigonometric parameter is set to $\beta = 3\pi/2$ so that $\cos(3\pi\hat{x}_1/2)$ and $\sin(3\pi\hat{x}_1/2)$ belong to the space used in the $\hat{x}_1$ direction. Consequently, the geometric map $\mathbf{F}$ is a member of $\widehat{\mathbb{X}}_h^0 \times \widehat{\mathbb{X}}_h^0$ and the discretization is genuinely isogeometric on this annular domain. Such an exact representation of the circular geometry is not available for the purely polynomial B-spline complex.
- The exponential parameters are guided by the boundary-layer behavior of advection-dominated flow. Since the advecting field $\mathbf{U} = (-\sin\theta, \cos\theta)$ is the unit azimuthal vector, advection takes place in the angular direction with unit speed, and the relevant one-dimensional model along a circle of radius r is the advection–diffusion equation $-\nu\,\partial_s^2\phi + \partial_s\phi = g$ in the arc-length variable s, whose homogeneous solutions are the constant 1 and the boundary-layer function $e^{s/\nu}$. Over the parametric coordinate $\hat{x}_1 \in [0, 1]$ the arc length at radius r equals $\frac{3\pi}{2} r\,\hat{x}_1$, so the layer is captured by $e^{\alpha\hat{x}_1}$ with rate $\alpha = -\frac{3\pi}{2} r/\nu$ (the sign being fixed by the advection direction). Sampling the three representative radii of the annulus – the inner boundary ($r = 1$), the mid-radius ($r = 3/2$), and the

outer boundary ($r = 2$) – yields $\alpha_1 = -\frac{3\pi}{2\nu}$, $\alpha_2 = -\frac{9\pi}{4\nu}$, and $\alpha_3 = -\frac{3\pi}{\nu}$. For bi-degree $(6, 6)$ these are exactly the three exponential terms that fit in the space once the constant, the linear term, and the trigonometric pair are accounted for.

All these values are dictated directly by the geometry and the data of the problem, and involve no fitting to the computed solution; they are chosen *a priori*, following the strategy adopted in [21].

As can be seen, the Tchebycheffian splines yield a significantly more accurate approximation than their polynomial counterparts. In particular, the Tchebycheffian spline solution is already quite accurate on the coarsest mesh and refinement leads to better resolution of the boundary layer. The polynomial spline solutions, on the other hand, are not very accurate on coarse meshes and show non-physical oscillations, still visible on the finest mesh.

6. Conclusion

We have presented and analyzed discretizations of differential forms based on Tchebycheffian splines whose different pieces are taken from nullspaces of constant-coefficient linear differential operators. Our results fully extend those in [3,4].

The cornerstone of this extension is the complete structural similarity between Tchebycheffian splines (and Tchebycheffian B-splines) and their polynomial counterparts, stemming from the fact that Tchebycheff spaces represent the most natural extension of polynomial spaces. This similarity encompasses key aspects such as derivative behavior, approximation properties, and existence of suitable projectors, which make it possible to construct commuting de Rham diagrams in two and three spatial dimensions, closely mirroring the polynomial case.

A full Tchebycheffian spline theory is known for splines where the various pieces are drawn from different and general Tchebycheff spaces. However, in this paper we focus specifically on Tchebycheffian splines whose pieces belong to ECT-spaces that are nullspaces of constant-coefficient linear differential operators because they offer an effective balance between flexibility and computational performance for applications. In particular, in the context of isogeometric discretizations of differential forms, this class of Tchebycheffian splines has the following features.

- They offer a broad range of combinations of algebraic polynomial, exponential, and trigonometric functions equipped with a wide spectrum of shape parameters. Thus, they can feature more accurate approximations per degree of freedom whenever appropriate automatic, problem-driven selection strategies for the underlying ECT-spaces are applied.
- They enjoy both the ability of exact representation of conic sections of the rational model (NURBS) and the "closure" under differentiation of polynomials. This results in discretizations of differential forms in full alignment with the isogeometric paradigm, using the same functions to describe both the geometry and the unknown vector fields.
- They can be seamlessly integrated into any software library supporting polynomial B-splines thanks to efficient evaluation and manipulation routines that are available in a Matlab toolbox [17].

A particularly interesting extension of the presented construction involves discretizations based on Tchebycheffian splines that are piecewise drawn from potentially different Tchebycheff spaces (of the same dimension). If the involved Tchebycheff spaces all belong to the class of nullspaces of constant-coefficient linear differential operators, then this extension becomes straightforward whenever the conditions for the existence of a TB-spline basis are satisfied [21].

Further possible extensions of the present work include employing multi-degree Tchebycheffian splines [17,18] and local tensor-product structures for Tchebycheffian B-splines supporting local refinement, such as hierarchical Tchebycheffian B-splines [15] and locally refined Tchebycheffian B-splines [16]. In particular, it is expected that recent results on the construction of exact hierarchical B-spline de Rham complexes [7–10] can be directly used in the Tchebycheffian B-spline setting, since the key spline space properties that form the foundation of those results are preserved in the Tchebycheffian case. This would allow for the design of adaptive, structure-preserving isogeometric methods based on Tchebycheffian splines.

CRediT authorship contribution statement

Carla Manni: Writing – review & editing, Writing – original draft, Methodology, Investigation, Funding acquisition, Conceptualization; **Hendrik Speleers:** Writing – review & editing, Writing – original draft, Methodology, Investigation, Funding acquisition, Conceptualization; **Deepesh Toshniwal:** Writing – review & editing, Visualization, Software, Methodology, Investigation, Conceptualization.

Declaration of competing interest

The authors declare that they have no known competing financial interests or personal relationships that could have appeared to influence the work reported in this paper.

Acknowledgments

C. Manni and H. Speleers are members of the research group GNCS (Gruppo Nazionale per il Calcolo Scientifico) of INdAM (Istituto Nazionale di Alta Matematica). They acknowledge the MUR Excellence Department Project MatMod@TOV (CUP E83C23000330006) awarded to the Department of Mathematics of the University of Rome Tor Vergata. They are also partially supported by a Project of

Relevant National Interest (PRIN) under the National Recovery and Resilience Plan (PNRR) funded by the European Union – Next Generation EU (CUP E53D23017910001), by the Italian Research Center on High Performance Computing, Big Data and Quantum Computing (CUP E83C22003230001), and by a GNCS project (CUP E53C24001950001). The research of D. Toshniwal was partially supported by project number 202.150 awarded through the Veni research programme by the Dutch Research Council (NWO).

Data availability

No data was used for the research described in the article.

References

[1] D.N. Arnold, R.S. Falk, R. Winther, Finite element exterior calculus, homological techniques, and applications, Acta Numer. 15 (2006) 1–155.
[2] J.A. Cottrell, T.J.R. Hughes, Y. Bazilevs, Isogeometric Analysis: Toward Integration of CAD and FEA, John Whiley & Sons, 2009.
[3] A. Buffa, J. Rivas, G. Sangalli, R. Vázquez, Isogeometric discrete differential forms in three dimensions, SIAM J. Numer. Anal. 49 (2) (2011) 818–844.
[4] A. Buffa, G. Sangalli, R. Vázquez, Isogeometric analysis in electromagnetics: B-splines approximation, Comput. Methods Appl. Mech. Eng. 199 (2010) 1143–1152.
[5] L. Beirão da Veiga, A. Buffa, G. Sangalli, R. Vázquez, Mathematical analysis of variational isogeometric methods, Acta Numer. 23 (2014) 157–287.
[6] R.R. Hiemstra, D. Toshniwal, R.H.M. Huijsmans, M.I. Gerritsma, High order geometric methods with exact conservation properties, J. Comput. Phys. 257 (2014) 1444–1471.
[7] D.C. Cabanas, K.M. Shepherd, D. Toshniwal, R. Vázquez, Construction of exact refinements for the two-dimensional HB/THB-spline de Rham complex, (2025). arXiv preprint arXiv:2502.19542
[8] K. Dijkstra, C. Giannelli, D. Toshniwal, Macro-element refinement schemes for THB-splines: applications to Bézier projection and structure-preserving discretizations, Comput. Methods Appl. Mech. Eng. 452 (2026) 118707.
[9] J.A. Evans, M.A. Scott, K.M. Shepherd, D.C. Thomas, R. Vázquez Hernández, Hierarchical B-spline complexes of discrete differential forms, IMA J. Numer. Anal. 40 (1) (2020) 422–473.
[10] K. Shepherd, D. Toshniwal, Locally-verifiable sufficient conditions for exactness of the hierarchical B-spline discrete de Rham complex in $\mathbb{R}^n$, Found. Comput. Math. (2024) 1–43.
[11] S. Karlin, W.J. Studden, Tchebycheff Systems: with Applications in Analysis and Statistics, Interscience, New York, 1966.
[12] T. Lyche, C. Manni, H. Speleers, Tchebycheffian B-splines revisited: an introductory exposition, in: C. Giannelli, H. Speleers (Eds.), Advanced Methods for Geometric Modeling and Numerical Simulation, volume 35 of Springer INdAM series, Springer, Cham, 2019, pp. 179–216.
[13] M.-L. Mazure, Constructing totally positive piecewise Chebyshevian B-spline bases, J. Comput. Appl. Math. 342 (2018) 550–586.
[14] L.L. Schumaker, Spline Functions: Basic Theory, Cambridge University Press, 2007.
[15] C. Manni, F. Pelosi, H. Speleers, Local hierarchical *h*-refinements in IgA based on generalized B-splines, in: M. Floater, et al. (Eds.), Mathematical Methods for Curves and Surfaces, volume 8177 of Lecture notes in computer science, Springer, Berlin, Heidelberg, 2014, pp. 341–363.
[16] K. Raval, C. Manni, H. Speleers, Adaptive isogeometric analysis based on locally refined Tchebycheffian B-splines, Comput. Methods Appl. Mech. Eng. 430 (2024) 117186.
[17] H. Speleers, Algorithm 1020: computation of multi-degree Tchebycheffian B-splines, ACM Trans. Math. Softw. 48 (2022) 12.
[18] R.R. Hiemstra, T.J.R. Hughes, C. Manni, H. Speleers, D. Toshniwal, A Tchebycheffian extension of multidegree B-splines: algorithmic computation and properties, SIAM J. Numer. Anal. 58 (2020) 1138–1163.
[19] C. Manni, F. Pelosi, M.L. Sampoli, Generalized B-splines as a tool in isogeometric analysis, Comput. Methods Appl. Mech. Eng. 200 (2011) 867–881.
[20] C. Manni, A. Reali, H. Speleers, Isogeometric collocation methods with generalized B-splines, Comput. Math. Appl. 70 (2015) 1659–1675.
[21] K. Raval, C. Manni, H. Speleers, Tchebycheffian B-splines in isogeometric Galerkin methods, Comput. Methods Appl. Mech. Eng. 403 (2023) 115648.
[22] D.C. Cabanas, J. Dekker, A. Palha, D. Toshniwal, Mantis.jl: a structure-preserving finite element library, 2025, https://doi.org/10.5281/zenodo.17495870
[23] M.-L. Mazure, How to build all Chebyshevian spline spaces good for geometric design?, Numer. Math. 119 (2011) 517–556.
[24] M. Brilleaud, M.-L. Mazure, Design with L-splines, Numer. Algorithms 65 (2014) 91–124.
[25] H. Speleers, On the normalization of trigonometric and hyperbolic B-splines, Adv. Comput. Math. 51 (2025) 56.
[26] C.V. Beccari, G. Casciola, L. Romani, A practical method for computing with piecewise Chebyshevian splines, J. Comput. Appl. Math. 406 (2022) 114051.
[27] A. Ratnani, E. Sonnendrücker, An arbitrary high-order spline finite element solver for the time domain Maxwell equations, J. Sci. Comput. 51 (2012) 87–106.
[28] W.L. Burke, Applied Differential Geometry, Cambridge University Press, 1985.
[29] L. Bruni Bruno, E. Zampa, Unisolvent and minimal physical degrees of freedom for the second family of polynomial differential forms, ESAIM Math. Model. Numer. Anal. 56 (6) (2022) 2239–2253.
[30] B. Kapidani, R. Vázquez, High order geometric methods with splines: an analysis of discrete Hodge-star operators, SIAM J. Sci. Comput. 44 (6) (2022) A3673–A3699.
[31] R. Hiptmair, Discrete Hodge operators, Numer. Math. 90 (2) (2001) 265–289.
[32] A. Buffa, J. Corno, C. de Falco, S. Schöps, R. Vázquez Hernández, Isogeometric mortar coupling for electromagnetic problems, SIAM J. Sci. Comput. 42 (1) (2020) B80–B104.
[33] D. Boffi, Finite element approximation of eigenvalue problems, Acta Numer. 19 (2010) 1–120.
[34] C. Garoni, H. Speleers, S.-E. Ekström, A. Reali, S. Serra-Capizzano, T.J.R. Hughes, Symbol-based analysis of finite element and isogeometric B-spline discretizations of eigenvalue problems: exposition and review, Arch. Comput. Methods Eng. 26 (5) (2019) 1639–1690.
[35] L. Bruni Bruno, M. Semplice, S. Serra-Capizzano, The numerical linear algebra of weights. Part I: from the spectral analysis to conditioning and preconditioning in the one-dimensional Laplacian case, BIT Numer. Math. 65 (4) (2025) 46.
[36] M.L. Cardinali, C. Garoni, C. Manni, H. Speleers, Isogeometric discretizations with generalized B-splines: symbol-based spectral analysis, Appl. Numer. Math. 166 (2021) 288–312.
[37] F. Roman, C. Manni, H. Speleers, Spectral analysis of matrices in Galerkin methods based on generalized B-splines with high smoothness, Numer. Math. 135 (1) (2017) 169–216.